An Approximate Maximum Likelihood Method for the Joint Estimation of Range and Doppler of Multiple Targets in OFDM-Based Radar Systems

Michele Mirabella, Pasquale Di Viesti, *Student Member, IEEE*, Alessandro Davoli, *Student Member, IEEE* and Giorgio M. Vitetta, *Senior Member, IEEE*

Abstract

In this manuscript, an innovative method for the detection and the estimation of multiple targets in a radar system employing orthogonal frequency division multiplexing is illustrated. The core of this method is represented by a novel algorithm for the detection of multiple superimposed two-dimensional complex tones in the presence of noise and the for estimation of their parameters. This algorithm is based on a maximum likelihood approach and combines a single tone estimator with a serial cancellation procedure. Our numerical results lead to the conclusion that the developed method can achieve a substantially better accuracy-complexity trade-off than various related techniques in the presence of closely spaced targets.

Index terms— Maximum likelihood estimation, frequency estimation, dual-function radar-communication, spectral analysis, radar processing, orthogonal frequency division multiplexing, joint communication and sensing, harmonic retrieval.

I. Introduction

Wireless communication and radar sensing have been advancing independently for many years, even though they share various similarities in terms of both signal processing and system architecture. During the last few years, substantial research efforts have been devoted to the design of wireless systems able to perform *communication and radar* (C&R) functions jointly. The interest in this class of systems, collectively known as *joint communication and sensing* (JCAS or JC&S), *integrated sensing and communication* (ISAC) or *dual functional radar communication* (DFRC), has been motivated by the advantages they offer in term of device size, power consumption, cost and efficiency radio spectrum usage with respect to traditional wireless systems. The initial studies in this field date back to the sixties, when the development of multi-function military radars was investigated [1]. More recently, substantial attention to JCAS has been paid by both academia and industry, thanks to its great potential in emerging defence applications, smart cities, as well as in intelligent vehicular networks [2].

Communication-centric, *radar centric joint design and optimization* approaches to JCAS design are currently being investigated in the technical literature [1], [3], [4]. On the one hand, in *communication-centric* design, radar sensing can be considered as an add-on to a given communication system, since priority is given to the communication function; for this reason, communication waveforms are exploited to extract radar information from target echoes. On the other hand, the *radar centric* approach aims at modulating (or incorporating information signalling in) a known radar waveform, thus leaving radar capability largely unaltered; its main drawback is represented by the fact that limited data rates are achievable. The third approach, namely *joint design and optimization*, offers a tunable trade-off between communication and sensing.

In the remaining part of this manuscript we focus on a *communication-centric* approach. More specifically, we take into consideration a JCAS system employing a single transmit and a single receive antenna, and a multicarrier modulation format known as *ortogonal frequency division multiplexing* (OFDM); this format has been adopted in various wireless communication standards, thanks to its robustness to multipath fading and its relatively simple synchronization [4]. In the technical literature, *direct* and *indirect sensing* methods for target detection and estimation are available for OFDM-based JCAS systems. In general, *direct sensing methods* extract target information from the received signal without compensating for the effect of the data payload it conveys [1] and typically exploit computationally intensive *compressed sensing* (CS) techniques. *Indirect estimation methods*, instead, require estimating the communication channel and, consequently, compensating for the contribution due to channel symbols (e.g., see [5, eq. (8)]).

Various direct methods can be found in [6]–[8] and in [9], where on-grid and off-grid CS techniques, and an atomic norm minimization method, respectively, have been investigated. A wider literature is available on indirect methods, that can be divided in: a) *discrete Fourier transform* (DFT)-based or *correlation-based* methods (i.e., methods based on the *matched filter*, MF, concept); b) subspace methods; c) *maximum likelihood* (ML) based methods. Moreover, subspace methods can be

The authors are with the University of Modena and Reggio Emilia, Dept. of Engineering "Enzo Ferrari", Via P. Vivarelli 10/1, 41125 Modena (Italy) and with Consorzio Nazionale Interuniversitario per le Telecomunicazioni (CNIT), email: michele.mirabella@unimore.it, pasquale.diviesti@unimore.it, alessandro.davoli@unimore.it, giorgio.vitetta@unimore.it.

further divided in *statistical* algorithms, like the *Multiple Signal Classification* (MUSIC) algorithm and the *estimation of signal parameters via rotational invariant techniques* (ESPRIT), and *deterministic* estimators, such as the Capon beamformer method [10], the *amplitude and phase estimation of a sinusoid* (APES) [11]–[13] and the *iterative adaptive approach for amplitude and phase estimation* (IAA-APES) [14].

Correlation-based and DFT-based methods have been proposed in [15]–[24]. More specifically, different MF-based techniques for estimating range and Doppler in a single or multi-target scenario have been devised in [15], [24]. These techniques exploit the prior knowledge of the received signal and, even if conceptually simple, are not computationally efficient; in addition, they may generate poor radar images because of the presence of high sidelobes and leakage, especially in the presence of strong clutter around real targets [25]. Methods for mitigating the last problem have been illustrated in [18] and [26]. Moreover, a reduced complexity method, based on the idea of splitting a *two-dimensional* (2D) estimation problem (involving target range and Doppler) into a couple of *one-dimensional* (1D) simpler sub-problems has been illustrated in [21].

Subspace methods for target range and Doppler estimation have been developed in [9], [27], [28] and [29]. In particular, MUSIC-based algorithms have been proposed in [9], [27] and [28], whereas the use of the ESPRIT technique for the estimation of the delay and Doppler of multiple targets has been investigated in [29]. Research work in this area has led to the conclusion that estimation techniques based on the 2D-MUSIC algorithm can outperform 2D fast Fourier transform (FFT)-based methods for joint range-velocity estimation at the price, however, of a significantly larger computational complexity [27]. A lower complexity version of the MUSIC technique, called *auto-paired method*, has been developed in [28]; it exploits the translational invariance structure of the underlying signal model in both frequency and time domains to reduce the size of the search space. Moreover, an iterative method able to improve the robustness of the MUSIC algorithm has been proposed in [9]; in this case, the channel frequency response is estimated through a standard method, known as *alternating direction of multipliers*, and a conventional 2D-MUSIC algorithm is employed for the estimation of target delays and Doppler frequencies.

A resolution comparable to that of subspace methods can be achieved through various ML-based algorithms at the price of an increase in computational complexity [30]–[34]. Research work in this field concerns: a) the use of the *amplitude weighted linearly constrained minimum variance* (AW-LCMV) method for estimating the parameters of multiple targets [30]; b) the adoption of an *alternating maximization* (AM) approach to mitigate the computational complexity of ML estimation [31]; c) the development of an iterative non-linear *kernel least mean square* (KLMS) based estimation technique for the estimation of target range [32]; d) the derivation of a ML method, based on a kinematic model of detected targets, for estimating target speed [34].

In this manuscript, a novel approximate ML-based algorithm for detecting multiple targets and jointly estimating their range and Doppler in an OFDM-based radar system is derived. This algorithm, called *complex single frequency-delay estimation and cancellation* (CSFDEC), combines an iterative DFT-based algorithm, developed for the ML estimation of a single 2D complex tone and called *complex single frequency-delay estimation* (CSFDE), with a serial cancellation & refinement procedure.

The relevant features of the CSFDEC algorithm originate from the fact that: a) the CSFDE algorithm, through the evaluation of multiple *symplectic Fourier transforms* (SFTs), is able to detect and accurately estimate the parameters of single complex 2D tones even in the presence of the *leakage* due to nearby tones; b) the adopted serial cancellation & refinement procedure is accurate and mathematically simple (in particular, unlike ML-based and subspace methods, does not require matrix inversions and eigendecompositions). In fact, for these reasons, the CSFDEC requires a limited computational effort, achieves good accuracy, and is able to detect and estimate closely spaced targets in scenarios in which DFT-based methods, subspace methods and other ML-based methods fail.

The remaining part of this manuscript is organized as follows. In Section II, the processing accomplished in an OFDM-based radar system is summarised and the model of the signal feeding the CSFDEC algorithm is briefly derived. Section III is devoted to the derivation of the CSFDE and CSFDEC algorithms, and to the assessment of their computational complexity. Other estimators available in the technical literature are described in Section IV. All the considered estimation algorithms are compared in terms of accuracy and complexity in Section V. Finally, some conclusions are offered in Section VI.

II. System and Signal Models

This section focuses on the processing accomplished at the receive side of a *single-input single output* (SISO) OFDM-based radar system; our main objectives are deriving the mathematical model of the received signal in the presence of multiple targets and illustrating some essential assumptions on which it relies. In the following, we take into consideration the transmission of a single frame, consisting of M consecutive OFDM symbols. The complex envelope of the transmitted signal conveying the

m-th OFDM symbol (with $m = 0, 1, \ldots, M-1$) of the considered frame can be expressed as (e.g., see [31, eq. (3)])

$$x_m(t) \triangleq x(t - mT_s) = q(t - mT_s) \cdot \sum_{n=0}^{N-1} s_m(n) \exp(j2\pi n\Delta_f (t - mT_s)), \tag{1}$$

where $q(t)$ is a windowing function, $s_m(n)$ is the channel symbol carried by the n-th subcarrier of the m-th OFDM symbol (with $n = 0, 1, \ldots, N-1$), N is the overall number of subcarriers, $\Delta_f = 1/T$ is the subcarrier spacing, T is the OFDM symbol interval,

$$T_s \triangleq T + T_G \tag{2}$$

is the overall duration of the OFDM symbol and T_G is the *cyclic prefix* duration (also known as *guard time* [3]); following [31], the rectangular windowing function

$$q(t) \triangleq \begin{cases} 1 & \text{for } t \in [-T_G, T] \\ 0 & \text{elsewhere} \end{cases} \tag{3}$$

is assumed in this manuscript. Given the complex envelope (1), the *radio frequency* (RF) waveform radiated by the radar transmitter can be expressed as

$$x_{RF}(t) = \Re\left\{ \exp(j2\pi f_c t) \sum_{m=0}^{M-1} x(t - mT_s) \right\}, \tag{4}$$

where f_c denotes the frequency of the local oscillator employed in the up-conversion at the transmit side. Let assume now that the last waveform is reflected by a single point target, located at the (initial) distance R from the transmitter and moving at the radial velocity[1] v with respect to it. It is not difficult to show that, in this case, the complex envelope of the signal received by the JCAS system is (e.g., see [31, eq. (6)])

$$r(t) = \exp(-j2\pi f_c \tau) \exp(j2\pi f_D t) \cdot \sum_{m=0}^{M-1} x\left(t - mT_s - \tau + \frac{f_D}{f_c} t \right) + w(t), \tag{5}$$

where

$$\tau \triangleq \frac{2R}{c} \tag{6}$$

is the overall propagation delay,

$$f_D = 2\frac{v}{\lambda} \tag{7}$$

is the Doppler shift due to target motion, $\lambda = c/f_c$ is the wavelength of the radiated signal and $w(t)$ is the complex *additive Gaussian noise* (AGN) process affecting $r(t)$.

The signal $r(t)$ (5) undergoes analog-to-digital conversion followed by DFT processing. A simple mathematical model describing the sequence generated by the sampling of $r(t)$ can be derived as follows. Substituting the *right-hand side* (RHS) of (1) in that of (5) and extracting the portion associated with the m-th OFDM symbol from the resulting expression yields

$$r_m(t') = A(\tau) \exp(j2\pi f_D t') \exp(j2\pi f_D m T_s) \cdot \sum_{n=0}^{N-1} s_m(n)\, \gamma_n(\tau)\, \xi_n(f_D, t') \cdot \zeta_{m,n}(f_D) \exp(j2\pi n\Delta_f\, t') + w(t'), \tag{8}$$

where

$$t' \triangleq t - mT_s, \tag{9}$$

$$A(\tau) \triangleq \exp(-j2\pi f_c \tau), \tag{10}$$

$$\gamma_n(\tau) \triangleq \exp(-j2\pi n\Delta_f \tau), \tag{11}$$

$$\xi_n(f_D, t') \triangleq \exp\left(j2\pi n\Delta_f \frac{f_D}{f_c} t' \right) \tag{12}$$

and

$$\zeta_{m,n}(f_D) \triangleq \exp\left(j2\pi n\Delta_f \frac{f_D}{f_c} m T_s \right). \tag{13}$$

[1]This velocity is positive (negative) if the target approaches (moves away from) the considered radar system.

Note that: a) the phase of $A(\tau)$ (10) depends on the target delay τ only, whereas that of $\gamma_n(\tau)$ (11) is proportional to both τ and the subcarrier index n; c) $\xi_n(f_D, t')$ (12) produces a time-dependent phase rotation depending on both the target speed v and the subcarrier index n; d) $\zeta_{m,n}(f_D)$ (13) generates a phase rotation depending on both the OFDM symbol index m and the subcarrier index n, and accounts for the so called *intersubcarrier Doppler effect* (see [31, Sec. II, p. 3]).

Based on (8), it is not difficult to show that, if $|f_D T_G| \ll 1$ and $|f_D \tau| \ll 1$, sampling $r_m(t')$ (8) at the instant

$$t'_{m,l} = \tau + T_G + \frac{T}{N} l, \tag{14}$$

with $l = 0, 1, ..., N-1$, yields

$$\begin{aligned} r_m(l) \triangleq r_m\big(t'_{m,l}\big) = A(\tau) \exp\left(j2\pi \frac{l}{N} \frac{f_D}{\Delta_f}\right) \exp(j2\pi f_D m T_s) \\ \cdot \sum_{n=0}^{N-1} s_m(n)\, \gamma_n(\tau)\, \xi_{n,l}(f_D)\, \zeta_{m,n}(f_D) \\ \cdot \exp\left(j2\pi n \frac{l}{N}\right) + w_m(l), \end{aligned} \tag{15}$$

where $\xi_{n,l}(f_D) \triangleq \xi_n(f_D, Tl/N)$ and $w_m(l) \triangleq w(t'_{m,l})$ is the Gaussian noise affecting $r_m(l)$. In the following, we also assume that: a) the sequence $\{w_m(l);\, l = 0, 1, ..., N-1\}$ can be modelled as *additive white Gaussian noise* (AWGN); b) the target speed is limited, so that

$$\left|\frac{2v}{c}\right| \ll \frac{1}{MN} \tag{16}$$

and

$$\frac{|f_D|}{\Delta_f} = |f_D T| \ll 1. \tag{17}$$

Consequently, the factors $\exp(j2\pi(lf_D)/(N\Delta_f))$, $\xi_{n,l}(f_D)$, $\zeta_{m,n}(f_D)$ appearing in the RHS of (15) can be neglected; this leads to the simplified signal model

$$\begin{aligned} r_m(l) = A(\tau) \exp(j2\pi f_D m T_s) \sum_{n=0}^{N-1} s_m(n)\, \gamma_n(\tau) \\ \cdot \exp\left(j2\pi n \frac{l}{N}\right) + w_m(l), \end{aligned} \tag{18}$$

that represents our reference model.

The N signal samples acquired in the m-th OFDM symbol interval are collected in the vector

$$\mathbf{r}_m \triangleq [r_m(0),\ r_m(1), ..., r_m(N-1)]^T, \tag{19}$$

that undergoes order N DFT processing. The n-th element of the resulting DFT output vector

$$\mathbf{R}_m \triangleq [R_m(0),\ R_m(1), ..., R_m(N-1)]^T \tag{20}$$

is

$$\begin{aligned} R_m(n) &\triangleq \frac{1}{N} \sum_{l=0}^{N-1} r_m(l) \exp\left(-j2\pi \frac{nl}{N}\right) \\ &= A(\tau) \exp(j2\pi f_D m T_s)\, s_m(n) \\ &\quad \cdot \exp(-j2\pi n \Delta_f \tau) + W_m(n), \end{aligned} \tag{21}$$

where $W_m(n)$ is the Gaussian noise affecting the n-th subcarrier of m-th OFDM symbol. Since the channel symbol $s_m(n)$ is known at the receive side for any n and m, the estimate

$$\hat{H}_{m,n} \triangleq \frac{R_m(n)}{s_m(n)} = A(\tau)\, M_{m,n}(F_D, F_r) + \bar{W}_m(n) \tag{22}$$

of the channel frequency response $H_{m,n}$ at the n-th subcarrier frequency in the m-th OFDM symbol interval can be computed; here,

$$F_r \triangleq \Delta_f\, \tau \tag{23}$$

is the *normalised target delay*,

$$F_D \triangleq f_D T_s \tag{24}$$

is the *normalised Doppler frequency*[2],

$$M_{m,n}(F_D, F_r) \triangleq a_m(F_D)\, b_n(F_r), \tag{25}$$

$$a_m(F_D) \triangleq \exp(j2\pi m F_D), \tag{26}$$

$$b_n(F_r) \triangleq \exp(-j2\pi n F_r) \tag{27}$$

and

$$\bar{W}_m(n) \triangleq \frac{W_m(n)}{s_m(n)} \tag{28}$$

is the noise sample affecting $\hat{H}_{m,n}$ (22).

It is worth noting that:

1) The parameter F_r (23) (F_D (24)) satisfies the inequalities $F_{r,\min} \leqslant F_r \leqslant F_{r,\max,}$ ($F_{D,\min} \leqslant F_D \leqslant F_{D,\max}$), with $F_{r,\min} = 0$ and $F_{r,\max} = 1$ ($F_{D,\min} = -1/2$ and $F_{D,\max} = 1/2$).
2) An AWGN model is usually adopted for the noise samples $\{W_m(n)\}$ (see (21)); however, in principle, this model does not hold for the noise samples $\{\bar{W}_m(n)\}$ (see (28)), unless the channel symbols $\{s_m(n)\}$ belong to a *phase shift keying* (PSK) constellation, as pointed out in [27, Sec. IV A]. In our computer simulations, a PSK constellation has been always used and each element of the set $\{\bar{W}_m(n)\}$ has been assumed to have zero mean and variance σ_W^2.
3) Without any loss of generality, the term $A(\tau)$ appearing in the RHS of (22) can be replaced by the complex gain

$$A \triangleq a \exp(j\phi), \tag{29}$$

that accounts for: 1) the phase rotation due to τ; 2) the path loss; 3) the gain (attenuation) introduced by the target.

The model (22) has been derived for a single target, but can be easily generalised to the case of K point targets. In fact, in the last case, we have that

$$\hat{H}_{m,n} \triangleq \sum_{k=0}^{K-1} A_k\, M_{m,n}(F_{D_k}, F_{r_k}) + \bar{W}_m(n), \tag{30}$$

where F_{r_k}, F_{D_k} and A_k represent the normalised delay, the normalised Doppler frequency and the complex gain, respectively, characterising the k-th target.

From (30) it can be easily inferred that: a) the noisy samples $\{\hat{H}_{m,n}\}$ of the 2D channel response acquired over a single frame can be modelled as the superposition of multiple 2D complex exponentials with AWGN; b) target detection and estimation is tantamount to identifying the K complex exponentials forming the useful component of the sequence $\{\hat{H}_{m,n}\}$ and estimating their parameters.

III. Approximate Maximum Likelihood Estimation of Two-Dimensional Complex Tones

In this section, we first derive a novel algorithm for jointly estimating the parameters of a single 2D complex tone. Then, we show how this algorithm can be exploited to detect multiple superimposed tones and estimate their parameters through a procedure based on successive cancellations and refinements. Finally, we analyse the computational complexity of the developed algorithms.

A. Joint estimation of the parameters of a single two-dimensional complex tone

Let us focus on the problem of estimating the parameters of a single 2D complex tone affected by AGN on the basis of the noisy observations $\{\hat{H}_{m,n}\}$, where (e.g., see (22) or (30) with $K = 1$)

$$\hat{H}_{m,n} = A \exp(j2\pi m F_D) \exp(-j2\pi n F_r) + \bar{W}_m(n), \tag{31}$$

with $m = 0,\ 1,\ ...,\ M-1$ and $n = 0,\ 1,\ ...,\ N-1$; here, the parameters A, F_D, F_r and $\bar{W}_m(n)$ represent the complex amplitude, the normalized Doppler frequency, the normalized delay and the noise affecting the n-th subcarrier of the m-th OFDM symbol, respectively. If we assume that the noise samples $\{\bar{W}_m(n)\}$ have the same variance, the ML estimates $F_{D,\mathrm{ML}}$, $F_{r,\mathrm{ML}}$ and A_{ML} of F_D, F_r and A, respectively, can be evaluated as

$$(F_{D,\mathrm{ML}}, F_{r,\mathrm{ML}}, A_{\mathrm{ML}}) \triangleq \arg \min_{\tilde{F}_D, \tilde{F}_r, \tilde{A}} \varepsilon\Big(\tilde{F}_D, \tilde{F}_r, \tilde{A}\Big), \tag{32}$$

where $\tilde{F}_D$, $\tilde{F}_r$ and $\tilde{A}$ are the trial values of F_D, F_r and A, respectively,

$$\varepsilon\Big(\tilde{F}_D, \tilde{F}_r, \tilde{A}\Big) \triangleq \frac{1}{M}\frac{1}{N} \sum_{m=0}^{M-1} \sum_{n=0}^{N-1} \varepsilon_{m,n}\Big(\tilde{F}_D, \tilde{F}_r, \tilde{A}\Big) \tag{33}$$

[2]Note that F_r is always a positive quantity, whereas F_D is positive (negative) if the considered target is approaching (moving away from) the radar.

is the *mean square error* (MSE) computed over the whole set $\{\hat{H}_{m,n}\}$,

$$\varepsilon_{m,n}\Big(\tilde{F}_D,\tilde{F}_r,\tilde{A}\Big) \triangleq \Big|\hat{H}_{m,n}-H_{m,n}\Big(\tilde{F}_D,\tilde{F}_r,\tilde{A}\Big)\Big|^2 \tag{34}$$

is the *square error* between the noisy sample $\hat{H}_{m,n}$ (31) and its useful component

$$H_{m,n}\Big(\tilde{F}_D,\tilde{F}_r,\tilde{A}\Big) \triangleq \tilde{A}\exp\Big(j2\pi m\tilde{F}_D\Big)\exp(-j2\pi n\tilde{F}_r) \tag{35}$$

evaluated under the assumption that $F_D=\tilde{F}_D$, $F_r=\tilde{F}_r$ and $A=\tilde{A}$. Substituting the RHS of the last equation in that of (34) yields

$$\begin{aligned}\varepsilon_{m,n}\ \Big(\tilde{F}_D,\tilde{F}_r,\tilde{A}\Big) &= \big|\hat{H}_{m,n}\big|^2+\big|\tilde{A}\big|^2\\ &-2\Re\Big\{\hat{H}_{m,n}\ \tilde{A}^*\exp\Big(-j\Big(\tilde{\varphi}_m-\tilde{\phi}_n\Big)\Big)\Big\},\end{aligned} \tag{36}$$

where

$$\tilde{\varphi}_m \triangleq 2\pi m\tilde{F}_D \tag{37}$$

and

$$\tilde{\phi}_n \triangleq 2\pi n\tilde{F}_r. \tag{38}$$

Then, substituting the RHS of (36) in that of (33) yields, after some manipulation,

$$\varepsilon\Big(\tilde{F}_D,\tilde{F}_r,\tilde{A}\Big)=\varepsilon_H+\big|\tilde{A}\big|^2-2\Re\Big\{\tilde{A}^*\bar{Y}\Big(\tilde{F}_D,\tilde{F}_r\Big)\Big\}, \tag{39}$$

where

$$\varepsilon_H \triangleq \frac{1}{M\,N}\sum_{m=0}^{M-1}\sum_{n=0}^{N-1}\big|\hat{H}_{m,n}\big|^2 \tag{40}$$

and

$$\begin{aligned}\bar{Y}\Big(\tilde{F}_D,\tilde{F}_r\Big) &\triangleq \frac{1}{M\,N}\mathrm{SFT}\Big[\hat{H}_{m,n}\Big]\\ &\triangleq \frac{1}{M\,N}\sum_{m=0}^{M-1}\sum_{n=0}^{N-1}\hat{H}_{m,n}\ \exp\Big(j2\pi n\tilde{F}_r\Big)\\ &\quad\cdot\exp\Big(-j2\pi m\tilde{F}_D\Big)\end{aligned} \tag{41}$$

is, up to a scale factor, the so called *symplectic Fourier transform* (SFT) of the sequence $\{\hat{H}_{m,n}\}$.

From (39) it can be easily inferred that the optimization problem (32) does not admit a closed form solution because of the nonlinear dependence of $\varepsilon(\tilde{F}_D,\tilde{F}_r,\tilde{A})$ (39) on $\tilde{F}_D$ and $\tilde{F}_r$. However, an approximate solution to this problem can be derived by:

a) Expressing the dependence of the function $\varepsilon(\tilde{F}_D,\tilde{F}_r,\tilde{A})$ on the variables $\tilde{F}_D$ and $\tilde{F}_r$ through the couples $(F_{D,c}\,,\tilde{\delta}_D)$ and $(F_{r,c}\,,\tilde{\delta}_r)$ such that

$$\tilde{F}_D = F_{D,c}+\tilde{\delta}_D\,\bar{F}_D \tag{42}$$

and

$$\tilde{F}_r = F_{r,c}+\tilde{\delta}_r\,\bar{F}_r. \tag{43}$$

Here, $F_{D,c}$ ($F_{r,c}$) represents a *coarse estimate* of F_D (F_r), $\tilde{\delta}_D$ and $\tilde{\delta}_r$ are real variables called *residuals*, and

$$\bar{F}_D \triangleq 1/M_0 \tag{44}$$

and

$$\bar{F}_r \triangleq 1/N_0 \tag{45}$$

are the *normalised fundamental Doppler frequency* and the *normalised fundamental delay*, respectively, characterising the order (M_0,N_0) *discrete* SFT (DSFT)

$$\bar{\mathbf{Y}}_{0,0} \triangleq \big[\bar{Y}_{0,0}[l,p]\big] \tag{46}$$

of the zero padded version

$$\hat{\mathbf{H}}_{0,0}^{(\mathrm{ZP})} \triangleq \begin{bmatrix}\hat{\mathbf{H}}_{0,0} & \mathbf{0}_{M,(L_D-1)\,N}\\ \mathbf{0}_{(L_r-1)M,\,N} & \mathbf{0}_{(L_r-1)M,(L_D-1)\,N}\end{bmatrix} \tag{47}$$

of the $M\times N$ matrix

$$\hat{\mathbf{H}}_{0,0} \triangleq \Big[\hat{H}_{m,n}\Big], \tag{48}$$

that collects all the elements of the sequence $\{\hat{H}_{m,n}\}$; moreover, in the last equations, L_D and L_r are positive integers (dubbed *oversampling factors*), $\mathbf{0}_{D_1,D_2}$ is the $D_1 \times D_2$ null matrix,

$$M_0 \triangleq L_D\, M \tag{49}$$

and

$$N_0 \triangleq L_r\, N. \tag{50}$$

Note that the element (l,p) of $\bar{\mathbf{Y}}_{0,0}$ (46) is defined as

$$\begin{aligned}\bar{Y}_{0,0}[l,p] \triangleq \frac{1}{M_0 N_0} \sum_{m=0}^{M-1} \sum_{n=0}^{N-1} \hat{H}_{m,n}\, \exp\big(j2\pi np\bar{F}_r\big) \\ \cdot \exp\big(-j2\pi m\big(l\bar{F}_D - 1/2\big)\big),\end{aligned} \tag{51}$$

with $l = 0, 1, \dots M_0 - 1$ and $p = 0, 1, \dots N_0 - 1$.

b) Assuming that the residuals $\tilde{\delta}_D$ and $\tilde{\delta}_r$ (appearing in the RHS of (42) and (43), respectively) are small, so that the truncated Taylor series

$$\exp\big(j\tilde{X}\big) \simeq \sum_{k=0}^{3} \frac{j^k \tilde{X}^k}{k!}, \tag{52}$$

can be employed to approximate the dependence of the function $\varepsilon(\tilde{F}_D, \tilde{F}_r, \tilde{A})$ on these variables.

c) Exploiting an iterative method, known as *alternating minimization* (AM; e.g., see [35]) to minimise the approximate expression derived for $\varepsilon(\tilde{F}_D, \tilde{F}_r, \tilde{A})$; this allows us to transform the *three-dimensional* (3D) optimization (32) into a triplet of interconnected *one-dimensional* (1D) problems, each referring to a single parameter.

Let us show now how these principles can be put into practice. First of all, the exploitation of AM requires solving the following three sub-problems: **P1**) minimizing $\varepsilon(\tilde{F}_D, \tilde{F}_r, \tilde{A})$ with respect to $\tilde{A}$, given $\tilde{F}_D = \hat{F}_D$ and $\tilde{F}_r = \hat{F}_r$; **P2**) minimizing $\varepsilon(\tilde{F}_D, \tilde{F}_r, \tilde{A})$ with respect to $\tilde{F}_D$, given $\tilde{A} = \hat{A}$ and $\tilde{F}_r = \hat{F}_r$; **P3**) minimizing $\varepsilon(\tilde{F}_D, \tilde{F}_r, \tilde{A})$ with respect to $\tilde{F}_r$, given $\tilde{A} = \hat{A}$ and $\tilde{F}_D = \hat{F}_D$.

The first sub-problem can be solved exactly thanks to the polynomial dependence of the cost function $\varepsilon(\tilde{F}_D, \tilde{F}_r, \tilde{A})$ (39) on the variable $\tilde{A}$. In fact, the function $\varepsilon(\hat{F}_D, \hat{F}_r, \tilde{A})$ is minimized with respect to $\tilde{A}$ if[3]

$$\tilde{A} = \hat{A} = \bar{Y}\Big(\hat{F}_D, \hat{F}_r\Big), \tag{53}$$

where $\bar{Y}(\hat{F}_D, \hat{F}_r)$ can be computed exactly through its expression (41) or, in an approximate fashion, through a computationally efficient procedure based on the fact that the matrix

$$\bar{\mathbf{Y}}_s \triangleq L_D\, L_r\, \bar{\mathbf{Y}}_{0,0} \tag{54}$$

collects $M_0 \times N_0$ uniformly spaced samples of the function $\bar{Y}(\tilde{F}_D, \tilde{F}_r)$, since (see (41), (51), (49) and (50))

$$\bar{Y}_{0,0}[l,p] = \frac{1}{L_D\, L_r} \bar{Y}\big(l\bar{F}_D, p\bar{F}_r\big). \tag{55}$$

For this reason, if both the normalised frequencies $\hat{F}_D$ and $\hat{F}_r$ are different from a multiple of $\bar{F}_D$ (44) and $\bar{F}_r$ (45), respectively, an approximate evaluation of $\bar{Y}(\hat{F}_D, \hat{F}_r)$ can be accomplished by *interpolating*[4] the elements of the matrix $\bar{\mathbf{Y}}_s$ (54). Note also that the last matrix can be efficiently computed by performing an order N_0 *inverse* FFT (IFFT) along the rows of $\hat{\mathbf{H}}_{0,0}^{(\mathrm{ZP})}$ (47), followed an order M_0 FFT along the columns of the resulting matrix.

Let us take into consideration now the other two sub-problems. Such sub-problems, unlike the previous one, do not admit closed form solutions. However, approximate solutions can be developed by: a) representing the parameters F_D and F_r in the same form as $\tilde{F}_D$ (42) and $\tilde{F}_r$ (43), respectively, i.e. as $F_D = F_{D,c} + \delta_D\, \bar{F}_D$ and $F_r = F_{r,c} + \delta_r\, \bar{F}_r$; b) using the 2D periodogram method to estimate $F_{D,c}$ and $F_{r,c}$; c) devising a novel algorithm for estimating the residuals δ_D and δ_r, i.e. for accomplishing the *fine estimation* of F_D and F_r, respectively. The fine estimation algorithm is derived as follows. Based on the representations (42) and (43) of the trial variables $\tilde{F}_D$ and $\tilde{F}_r$, respectively, the variables $\tilde{\varphi}_m$ (37) and $\tilde{\phi}_n$ (38) are expressed as

$$\tilde{\varphi}_m = 2\pi m\, F_{D,c} + m\tilde{\Omega} \tag{56}$$

and

$$\tilde{\phi}_n = 2\pi n\, F_{r,c} + n\tilde{\Delta}, \tag{57}$$

[3]This is a generalisation of a well known result in the 1D case (e.g., see [36, Sec. IV]).

[4]See [37] for polynomial interpolation techniques or [38] for barycentric interpolation method.

respectively; here,

$$\tilde{\Omega} \triangleq 2\pi\tilde{\delta}_D\,\bar{F}_D \tag{58}$$

and

$$\tilde{\Delta} \triangleq 2\pi\tilde{\delta}_r\,\bar{F}_r. \tag{59}$$

Then, the following steps are accomplished: a) the RHSs of (56) and (57) are substituted in that of (36); b) the resulting expression is substituted in the RHS of (33) and the approximation (52) is adopted for $\exp(jm\tilde{\Omega})$ and $\exp(jn\tilde{\Delta})$ under the assumption that both $\tilde{\Omega}$ and $\tilde{\Delta}$ are small enough[5]. This yields, after some manipulation, the approximate expression

$$\varepsilon_{\mathrm{CSFDE}}\Big(\tilde{\Omega},\tilde{\Delta},\hat{A}\Big) \triangleq \varepsilon_H + \big|\hat{A}\big|^2 - 2\xi\Big(\tilde{\Omega},\tilde{\Delta},\hat{A}\Big) \tag{60}$$

for the function $\varepsilon(\tilde{F}_D,\tilde{F}_r,\tilde{A})$ (33); here,

$$\xi\Big(\tilde{\Omega},\tilde{\Delta},\hat{A}\Big) = \sum_{p=0}^{3}\sum_{q=0}^{3}(-1)^{(p+q)}\,\frac{\tilde{\Omega}^p\,\tilde{\Delta}^q}{p!q!}\,\Re\Big\{j^{(p-q)}\,\hat{A}^*\,\bar{Y}_{p,q}\Big\}, \tag{61}$$

$$\begin{aligned}\bar{Y}_{k_1,k_2}(\rho_D,\rho_r) \triangleq \frac{1}{MN}\sum_{m=0}^{M-1}\sum_{n=0}^{N-1}\hat{H}_{m,n}^{(k_1,k_2)}\,\exp\left(j\frac{2\pi n\rho_r}{N_0}\right)\\ \cdot\exp\left(-j\frac{2\pi m\rho_D}{M_0}\right),\end{aligned} \tag{62}$$

$$\rho_D \triangleq F_{D,c}/\bar{F}_D, \tag{63}$$

$$\rho_r \triangleq F_{r,c}/\bar{F}_r, \tag{64}$$

and

$$\hat{H}_{m,n}^{(k_1,k_2)} \triangleq m^{k_1}n^{k_2}\hat{H}_{m,n}, \tag{65}$$

with $m = 0,1,\ldots M-1$ and $n = 0,1,\ldots N-1$. It is important to point out that: a) if both ρ_D (63) and ρ_r (64) are integers, the quantity $\bar{Y}_{k_1,k_2}(\rho_D,\rho_r)$ (62) represents the element (ρ_D,ρ_r) of the $M_0\times N_0$ matrix

$$\bar{\mathbf{Y}}_{k_1,k_2} \triangleq \mathrm{DSFT}\Big[\hat{\mathbf{H}}_{k_1,k_2}^{(\mathrm{ZP})}\Big] \tag{66}$$

generated by the order (M_0,N_0) DSFT of the zero padded version

$$\hat{\mathbf{H}}_{k_1,k_2}^{(\mathrm{ZP})} \triangleq \begin{bmatrix}\hat{\mathbf{H}}_{k_1,k_2} & \mathbf{0}_{M,(L_D-1)\,N}\\ \mathbf{0}_{(L_r-1)M,\,N} & \mathbf{0}_{(L_r-1)M,(L_D-1)\,N}\end{bmatrix}; \tag{67}$$

of the $M\times N$ matrix $\hat{\mathbf{H}}_{k_1,k_2} \triangleq [\hat{H}_{m,n}^{(k_1,k_2)}]$; b) if the previous condition is not met, the quantity $\bar{Y}_{k_1,k_2}(\rho_D,\rho_r)$ can be evaluated exactly on the basis of (62) or, in an approximate fashion, by interpolating multiple adjacent elements of the matrix $L_D\,L_r\,\bar{\mathbf{Y}}_{k_1,k_2}$ (see (66)).

Minimising $\varepsilon_{\mathrm{CSFDE}}(\tilde{\Omega},\tilde{\Delta},\hat{A})$ (60) is equivalent to maximising the function $\xi(\tilde{\Omega},\tilde{\Delta},\hat{A})$ (61). The last function can be easily minimised with respect to the variable $\tilde{\Omega}$ ($\tilde{\Delta}$) if $\tilde{\Delta}$ ($\tilde{\Omega}$) is known. Therefore, given $\tilde{\Delta} = \hat{\Delta}$, the estimate

$$\hat{\delta}_D = \frac{\hat{\Omega}}{2\pi\bar{F}_D} \tag{68}$$

of δ_D can be evaluated by taking the derivative of $\xi(\tilde{\Omega},\hat{\Delta},\hat{A})$ with respect to $\tilde{\Omega}$ and setting it to zero. In fact, this leads to the estimate[6]

$$\hat{X} = \frac{-b_X + \sqrt{b_X^2 - 4\,a_X\,c_X}}{2\,a_X}, \tag{69}$$

that represents one of the two solutions of the quadratic equation

$$a_X\,\tilde{X}^2 + b_X\,\tilde{X} + c_X = 0, \tag{70}$$

with $X = \Omega$; here,

$$\begin{aligned}a_\Omega = -\frac{\hat{\Delta}^3}{6}\,\Re\Big\{\hat{A}^*\bar{Y}_{3,3}\Big\} - \frac{\hat{\Delta}^2}{2}\,\Im\Big\{\hat{A}^*\bar{Y}_{3,2}\Big\}\\ +\hat{\Delta}\,\Re\Big\{\hat{A}^*\bar{Y}_{3,1}\Big\} + \Im\Big\{\hat{A}^*\bar{Y}_{3,0}\Big\},\end{aligned} \tag{71}$$

[5]This is equivalent to assuming that $\bar{F}_D$ (44) and $\bar{F}_r$ (45) are small enough (i.e., M_0 and N_0 are large enough).

[6]In the following equations, the dependence of the function $\bar{Y}_{k_1,k_2}(\rho_D,\rho_r)$ (62) and of the coefficients $\{a_X,\,b_X,\,c_X\}$ on (ρ_D,ρ_r) is not explicitly specified to ease reading.

$$b_\Omega = \frac{\hat{\Delta}^3}{3}\Im\Big\{\hat{A}^*\bar{Y}_{2,3}\Big\} - \hat{\Delta}^2\,\Re\Big\{\hat{A}^*\bar{Y}_{2,2}\Big\} \\ -2\hat{\Delta}\,\Im\Big\{\hat{A}^*\bar{Y}_{2,1}\Big\} + 2\Re\Big\{\hat{A}^*\bar{Y}_{2,0}\Big\} \tag{72}$$

and

$$c_\Omega = \frac{\hat{\Delta}^3}{3}\Re\Big\{\hat{A}^*\bar{Y}_{1,3}\Big\} + \hat{\Delta}^2\,\Im\Big\{\hat{A}^*\bar{Y}_{1,2}\Big\} \\ -2\hat{\Delta}\,\Re\Big\{\hat{A}^*\bar{Y}_{1,1}\Big\} - 2\Im\Big\{\hat{A}^*\bar{Y}_{1,0}\Big\}. \tag{73}$$

A simpler estimate (denoted $\hat{\Omega}'$) of Ω is obtained neglecting the contribution of the quadratic term in the left-hand side (LHS) of (70), i.e. setting $a_\Omega = 0$. This leads to a first-degree equation, whose solution is

$$\hat{X}' = -c_X/b_X, \tag{74}$$

with $X = \Omega$.

Dually, given $\tilde{\Omega} = \hat{\Omega}$, the estimate

$$\hat{\delta}_r \triangleq \frac{\hat{\Delta}}{2\pi\bar{F}_r} \tag{75}$$

of $\tilde{\delta}_r$ is computed by taking the derivative of $\xi(\hat{\Omega}, \tilde{\Delta}, \hat{A})$ with respect to $\tilde{\Delta}$ and setting it to zero. This leads to a quadratic equation in the variable $\tilde{\Delta}$ whose structure is still expressed by (70) (with $X = \Delta$); however, its coefficients are

$$a_\Delta = -\frac{\hat{\Omega}^3}{6}\Re\Big\{\hat{A}^*\bar{Y}_{3,3}\Big\} + \frac{\hat{\Omega}^2}{2}\Im\Big\{\hat{A}^*\bar{Y}_{2,3}\Big\} \\ +\hat{\Omega}\,\Re\Big\{\hat{A}^*\bar{Y}_{1,3}\Big\} - \Im\Big\{\hat{A}^*\bar{Y}_{0,3}\Big\}, \tag{76}$$

$$b_\Delta = -\frac{\hat{\Omega}^3}{3}\Im\Big\{\hat{A}^*\bar{Y}_{3,2}\Big\} - \hat{\Omega}^2\,\Re\Big\{\hat{A}^*\bar{Y}_{2,2}\Big\} \\ +2\hat{\Omega}\,\Im\Big\{\hat{A}^*\bar{Y}_{1,2}\Big\} + 2\Re\Big\{\hat{A}^*\bar{Y}_{0,2}\Big\} \tag{77}$$

and

$$c_\Delta = \frac{\hat{\Omega}^3}{3}\Re\Big\{\hat{A}^*\bar{Y}_{3,1}\Big\} - \hat{\Omega}^2\,\Im\Big\{\hat{A}^*\bar{Y}_{2,1}\Big\} \\ -2\hat{\Omega}\,\Re\Big\{\hat{A}^*\bar{Y}_{1,1}\Big\} + 2\Im\Big\{\hat{A}^*\bar{Y}_{0,1}\Big\}. \tag{78}$$

For this reason, the estimates $\hat{\Delta}$ and $\hat{\Delta}'$ of Δ can be computed according to (69) and (74), respectively.

Given the estimates $\hat{\delta}_D$ (68) and $\hat{\delta}_r$ (75) (resulting from $\hat{\Omega}$ and $\hat{\Delta}$, or $\hat{\Omega}'$ and $\hat{\Delta}'$), a *fine estimate* $\hat{F}_D$ of F_D ($\hat{F}_r$ of F_r) can be evaluated on the basis of (42) ((43)).

The previous mathematical results allow us to easily develop an AM-based procedure for estimating the parameters F_D, F_r and A in an iterative fashion. This procedure, dubbed CSFDE, is initialised by computing: a) the $M_0 \times N_0$ matrices[7] $\{\bar{\mathbf{Y}}_{k_1,k_2}; k_1,\ k_2 = 0,1,2,3\}$ (see (66)); b) the coarse estimates

$$\hat{F}_{D,c}^{(0)} = \hat{l}\,\bar{F}_D - 1/2 \tag{79}$$

and

$$\hat{F}_{r,c}^{(0)} = \hat{p}\bar{F}_r \tag{80}$$

of F_D and F_r, respectively, where

$$\Big(\hat{l}, \hat{p}\Big) = \arg \max_{\tilde{l}\,\in\mathcal{S}_{M_0}, \tilde{p}\,\in\mathcal{S}_{N_0}} \Big\|\bar{Y}_{0,0}\Big[\tilde{l}, \tilde{p}\Big]\Big\|^2 \tag{81}$$

and $\mathcal{S}_X \triangleq \{0, 1, ..., X-1\}$ for any positive integer X; c) the initial estimate $\hat{A}^{(0)}$ of $\tilde{A}$ on the basis of (53), with $(\hat{F}_D, \hat{F}_r) = (\hat{F}_{D,c}^{(0)}, \hat{F}_{r,c}^{(0)})$; d) the coefficients $\{a_\Omega,\, b_\Omega,\, c_\Omega\}$ ($\{a_\Delta,\, b_\Delta,\, c_\Delta\}$) for $(\rho_D, \rho_r) = (\hat{l}^{(0)}, \hat{p}^{(0)})$) according to (72)-(73) ((76)-(78)); e) the initial estimate $\hat{\Omega}^{(0)}(\hat{\Delta}^{(0)})$ of Ω (Δ) on the basis of (69) or (74) with $X = \Omega$ (with $X = \Delta$); f) the initial fine estimates (see (42) and (43))

$$\hat{F}_D^{(0)} = \hat{F}_{D,c}^{(0)} + \frac{\hat{\Omega}^{(0)}}{2\pi} \tag{82}$$

[7]Note that the matrices $\{\bar{\mathbf{Y}}_{k_1,k_2}\}$ corresponding to $(k_1, k_2) = (0,3)$, $(3,0)$ and $(3,3)$ are not required if the simpler estimates $\hat{\Omega}'$ and $\hat{\Delta}'$ are evaluated.

and

$$\hat{F}_r^{(0)} = \hat{F}_{r,c}^{(0)} + \frac{\hat{\Delta}^{(0)}}{2\pi} \tag{83}$$

of F_D and F_r, respectively. Finally, we set the iteration index i to 1 and start an iterative procedure. The i-th iteration is fed by the estimates $\hat{F}_D^{(i-1)}$, $\hat{F}_r^{(i-1)}$ and $\hat{A}^{(i-1)}$ of F_D, F_r and A, respectively, and produces the new estimates $\hat{F}_D^{(i)}$, $\hat{F}_r^{(i)}$ and $\hat{A}^{(i)}$ of the same quantities (with $i = 1, 2, ..., N_{\rm it}$, where $N_{\rm it}$ is the overall number of iterations). The procedure adopted for the evaluation of $\hat{F}_D^{(i)}$, $\hat{F}_r^{(i)}$ and $\hat{A}^{(i)}$ consists of the two steps described below.

1) *Estimation of the normalised Doppler and the normalised delay* - The new estimates $\hat{\Omega}^{(i)}$ and $\hat{\Delta}^{(i)}$ of $\tilde{\Omega}$ and $\tilde{\Delta}$, respectively, are computed according to (69) or (74). In the evaluation of the coefficients of these equations, $\hat{A} = \hat{A}^{(i-1)}$,

$$\rho_D = \hat{\rho}_D^{(i-1)} = \hat{F}_D^{(i-1)} / \bar{F}_D \tag{84}$$

and

$$\rho_r = \hat{\rho}_r^{(i-1)} = \hat{F}_r^{(i-1)} / \bar{F}_r \tag{85}$$

are assumed. Then,

$$\hat{F}_D^{(i)} = \hat{F}_D^{(i-1)} + \frac{\hat{\Omega}^{(i)}}{2\pi} \tag{86}$$

and

$$\hat{F}_r^{(i)} = \hat{F}_r^{(i-1)} + \frac{\hat{\Delta}^{(i)}}{2\pi} \tag{87}$$

are computed.

2) *Estimation of the complex amplitude* - The new estimate $\hat{A}^{(i)}$ of $\hat{A}$ is evaluated by means of (53); in doing so, $\hat{F}_D = \hat{F}_D^{(i)}$ and $\hat{F}_r = \hat{F}_r^{(i)}$ are assumed.

The index i is incremented by one before starting the next iteration. At the end of the last (i.e. of the $N_{\rm it}$-th) iteration, the fine estimates $\hat{F}_D = \hat{F}_D^{(N_{\rm it})}$, $\hat{F}_r = \hat{F}_r^{(N_{\rm it})}$ and $\hat{A} = \hat{A}^{(N_{\rm it})}$ of F_D, F_r and A, respectively, become available. The CSFDE algorithm is summarized in Algorithm 1.

Algorithm 1: Complex single frequency-delay estimator (CSFDE)

Input: The matrices $\{\mathbf{Y}_{k_1,k_2}; k_1 = 0, 1, 2 \text{ and } 3;\ k_2 = 0, 1, 2 \text{ and } 3\}$ (see (66)) and the parameter $N_{\rm it}$.

Initialisation:

a- Evaluate $\bar{\mathbf{Y}}_{0,0}$ (46), $\hat{l}$ and $\hat{p}$ (see (81)); then, compute the initial estimate $\hat{A}^{(0)}$ of A according to (53) and set $(\rho_D^{(0)}, \rho_r^{(0)}) = (\hat{l}, \hat{p})$ (see (84)-(85)).

b- Compute the coefficients a_Ω, b_Ω and c_Ω according to (71)-(73); then, evaluate $\hat{\Omega}^{(0)}$ according to (69) or (74).

c- Evaluate the coefficients a_Δ, b_Δ and c_Δ according to (76)-(78); then, compute $\hat{\Delta}^{(0)}$ according to (69) or (74).

d- Compute $\hat{F}_D^{(0)}$ and $\hat{F}_r^{(0)}$ according to (82) and (83), respectively.

Refinement: for $i = 1$ *to* $N_{\rm it}$ **do**

e- *Estimation of* A:
Set $\hat{F}_D = \hat{F}_D^{(i-1)}$ and $\hat{F}_r = \hat{F}_r^{(i-1)}$; then, evaluate $\bar{Y}(\hat{F}_D, \hat{F}_r)$ using (41) or by interpolating a few adjacent elements of the matrix $\bar{\mathbf{Y}}_s$ (54). Finally, compute $\hat{A}^{(i)}$, $\hat{\rho}_D^{(i-1)}$ and $\hat{\rho}_r^{(i-1)}$ according to (53), (84) and (85), respectively.

f- *Estimation of* F_D:
Set $\hat{A} = \hat{A}^{(i)}$ and compute $\bar{Y}_{k_1,k_2}(\hat{\rho}_D^{(i-1)}, \hat{\rho}_r^{(i-1)})$ according to (62) or by interpolating a few adjacent elements of $\bar{\mathbf{Y}}_{k_1,k_2}$ (66); then, compute a_Ω, b_Ω and c_Ω according to (71)-(73) assuming $(\rho_D, \rho_r) = (\hat{\rho}_D^{(i-1)}, \hat{\rho}_r^{(i-1)})$. Finally, compute $\hat{\Omega}^{(i)}$ and $\hat{F}_D^{(i)}$ according to (69) or (74) and (86), respectively.

g- *Estimation of* F_r:
Compute $a_{\tilde{\Delta}}$, $b_{\tilde{\Delta}}$ and $c_{\tilde{\Delta}}$ according to (76)-(78) assuming $(\hat{\rho}_D^{(i-1)}, \hat{\rho}_r^{(i-1)})$; then, evaluate $\hat{\Delta}^{(i)}$ and $\hat{F}_r^{(i)}$ on the basis of (69) or (74) and (87), respectively.

end

Output: The estimates $\hat{F}_D^{(N_{\rm it})}$, $\hat{F}_r^{(N_{\rm it})}$ and $\hat{A}^{(N_{\rm it})}$ of F_D, F_r and A, respectively.

It is worth pointing out that: a) the initial coarse estimates $\hat{F}_{D,c}^{(0)}$ (82) and $\hat{F}_{r,c}^{(0)}$ (83) are computed by resorting to the 2D *periodogram method* (see (81)); b) unlike traditional DFT-based methods, the CSFDE algorithm requires the evaluation of multiple DSFTs and, more precisely, of 16 (13) DSFTs $\{\bar{\mathbf{Y}}_{k_1,k_2}\}$ if (69) ((74)) is employed in the evaluation of the estimates of Ω and Δ; c) the approximate ML metric $\varepsilon_{\rm CSFDE}(\tilde{\Omega}, \tilde{\Delta}, \hat{A})$ (60) on which the CSFDE algorithm is based is new; d) the estimates $\hat{\delta}_D^{(i)}$ ($\hat{\delta}_r^{(i)}$) of δ_D (δ_r) computed by the CSFDE algorithm in its i-th iteration are expected to become smaller as i increases, since $\hat{F}_D^{(i)}$ ($\hat{F}_r^{(i)}$) should progressively approach F_D (F_r) if this algorithm converges.

B. Estimation of multiple two-dimensional tones

Let us show now how the CSFDE algorithm can be exploited to recursively estimate the multiple tones forming the useful component of the complex sequence $\{\hat{H}_{m,n}\}$, whose (m,n)-th element is expressed by (30), where K is assumed to be greater than unity and *unknown*. The method we develop to achieve this objective is called *complex single frequency-delay estimation and cancellation* (CSFDEC) and is based on the following principles: a) tones are sequentially detected and estimated; b) the detection of a new tone and the estimation of its parameters are accomplished by the CSFDE algorithm; c) after detecting a new tone and estimating its parameters, a *re-estimation* technique is executed to improve the accuracy of both this tone and the previously estimated tones; d) recursions are stopped on the basis of a proper criterion, so that an estimate of K is also generated.

The CSFDEC algorithm is initialised by: 1) running the CSFDE algorithm to compute the initial estimates $\hat{F}_{D_0}^{(0)}$, $\hat{F}_{r_0}^{(0)}$ and $\hat{A}_0^{(0)}$ of the parameters F_{D_0}, F_{r_0} and A_0 characterising the first target; 2) setting the recursion index i to 1 and $\bar{\mathbf{Y}}_{0,0}^{(0)} = \bar{\mathbf{Y}}_{0,0}$ (see (46)). Then, a recursive procedure is started. The i-th recursion of this procedure is fed by the vectors

$$\hat{\mathbf{F}}_D^{(i-1)} = \left[\hat{F}_{D_0}^{(i-1)}, \hat{F}_{D_1}^{(i-1)}, ..., \hat{F}_{D_{i-1}}^{(i-1)}\right]^T, \tag{88}$$

$$\hat{\mathbf{F}}_r^{(i-1)} = \left[\hat{F}_{r_0}^{(i-1)}, \hat{F}_{r_1}^{(i-1)}, ..., \hat{F}_{r_{i-1}}^{(i-1)}\right]^T \tag{89}$$

and

$$\hat{\mathbf{A}}^{(i-1)} = \left[\hat{A}_0^{(i-1)}, \hat{A}_1^{(i-1)}, ..., \hat{A}_{i-1}^{(i-1)}\right]^T, \tag{90}$$

collecting the estimates of the normalised Doppler frequency, normalised delay and complex amplitude, respectively, of the i tones detected and estimated in the previous recursions, and generates the new vectors $\hat{\mathbf{F}}_D^{(i)}$, $\hat{\mathbf{F}}_r^{(i)}$ and $\hat{\mathbf{A}}^{(i)}$ after: a) estimating the parameters $\hat{F}_{D_i}^{(i)}$, $\hat{F}_{r_i}^{(i)}$ and $\hat{A}_i^{(i)}$ of the new (i.e., of the i-th) tone (if any); b) refining the estimates of the i tones available at the beginning of the considered recursion. The procedure employed for accomplishing all this consists of the three steps described below (the p-th step is denoted CSFDE-Sp, with $p = 1$, 2 and 3)

CSFDEC-S1 (*spectral cancellation and estimation of a new tone*) - In this step, the following quantities are evaluated (see the initialisation part of the CSFDE algorithm):

a) The *residual spectrum*

$$\begin{aligned}\mathbf{Y}_{0,0}^{(i)} = \left[\bar{Y}_{0,0}^{(i)}[l,p]\right] &\triangleq \mathbf{Y}_{0,0}^{(i-1)} \\ &-\mathbf{C}_{0,0}^{(i)}\left(\hat{\mathbf{A}}^{(i-1)}, \hat{\mathbf{F}}_D^{(i-1)}, \hat{\mathbf{F}}_r^{(i-1)}\right),\end{aligned} \tag{91}$$

where

$$\begin{aligned}&\mathbf{C}_{0,0}^{(i)}\left(\hat{\mathbf{A}}^{(i-1)}, \hat{\mathbf{F}}_D^{(i-1)}, \hat{\mathbf{F}}_r^{(i-1)}\right) \\ &\triangleq \sum_{k=0}^{i-1} \bar{\mathbf{C}}_{0,0}\left(\hat{A}_k^{(i-1)}, \hat{F}_{D_k}^{(i-1)}, \hat{F}_{r_k}^{(i-1)}\right)\end{aligned} \tag{92}$$

represents the contribution given by all the i-th estimated 2D tones to $\bar{\mathbf{Y}}_{0,0}$ and $\bar{\mathbf{C}}_{0,0}(\hat{A}_k^{(i-1)}, \hat{F}_{D_k}^{(i-1)}, \hat{F}_{r_k}^{(i-1)})$ is the contribution provided by the k-th tone (with $k = 0, 1, ..., i-1$) to the same matrix (the expression of the elements of the matrix $\bar{\mathbf{C}}_{0,0}(\cdot,\cdot,\cdot)$ is derived in Appendix A; see (169)). If the overall energy

$$\varepsilon_{0,0}[i] \triangleq \left\|\mathbf{Y}_{0,0}^{(i)}\right\|^2 \tag{93}$$

of the vector $\mathbf{Y}_{0,0}^{(i)}$ (91) satisfies the inequality

$$\varepsilon_{0,0}[i] < T_{\mathrm{CSFDEC}}, \tag{94}$$

where T_{CSFDEC} is a proper threshold, the algorithm stops and the estimate $\hat{K} = i$ of K is generated.

b) The couple of integers (see (81))

$$\left(\hat{l}^{(i)}, \hat{p}^{(i)}\right) = \arg \max_{\tilde{l} \in \mathcal{S}_{M_0}, \tilde{p} \in \mathcal{S}_{N_0}} \left|\bar{Y}_{0,0}^{(i)}\left[\tilde{l}, \tilde{p}\right]\right| \tag{95}$$

and the coarse estimates $\hat{F}_{D,c_i}^{(i)} = \hat{l}^{(i)}\bar{F}_D - 1/2$ and $\hat{F}_{r,c_i}^{(i)} = \hat{p}^{(i)}\bar{F}_r$ of $F_{D,c}$ and $F_{r,c}$, respectively (see (79) and (80)).

c) The preliminary estimate (see (53))

$$\begin{aligned}\bar{A}_i^{(i)} &= \bar{Y}(\hat{F}_{D,c_i}^{(i)}, \hat{F}_{r,c_i}^{(i)}) \\ &-\breve{Y}_{0,0}\left(\hat{F}_{D,c_i}^{(i)}, \hat{F}_{r,c_i}^{(i)}; \hat{\mathbf{A}}^{(i-1)}, \hat{\mathbf{F}}_D^{(i-1)}, \hat{\mathbf{F}}_r^{(i-1)}\right)\end{aligned} \tag{96}$$

of the complex amplitude A_i; here,

$$\begin{aligned}&\breve{Y}_{0,0}\Big(\hat{F}_{D,c_i}^{(i)}\,,\hat{F}_{r,c_i}^{(i)};\hat{\mathbf{A}}^{(i-1)},\hat{\mathbf{F}}_D^{(i-1)},\hat{\mathbf{F}}_r^{(i-1)}\Big)\\&\triangleq\sum_{k=0}^{i-1}\bar{Y}_{0,0}\Big(\hat{F}_{D,c_i}^{(i)}\,,\hat{F}_{r,c_i}^{(i)};\hat{A}_k^{(i-1)},\hat{F}_{D_k}^{(i-1)},\hat{F}_{r_k}^{(i-1)}\Big)\end{aligned}\tag{97}$$

is the contribution given to $\bar{Y}(\hat{F}_{D,c_i}^{(i)}\,,\hat{F}_{r,c_i}^{(i)})$ by the first i estimated tones for $(F_D\,,F_r)=(\hat{F}_{D,c_i}^{(i)}\,,\hat{F}_{r,c_i}^{(i)})$ and $\bar{Y}_{0,0}(\hat{F}_{D,c_i}^{(i)}\,,\hat{F}_{r,c_i}^{(i)};\hat{A}_k^{(i-1)},\hat{F}_{D_k}^{(i-1)},$ represents the leakage due to the k-th tone and affecting the i-th tone. The expression of the quantity $\bar{Y}_{k_1,k_2}(\hat{F}_{D,c_i}^{(i)}\,,\hat{F}_{r,c_i}^{(i)};\hat{A}_k^{(i-1)},\hat{F}_{D_k}^{(i-1)},\hat{F}_{r_k}^{(i-}$ is provided in Appendix B (see (174)).

d) The spectral coefficients

$$\begin{aligned}&\bar{Y}_{k_1,k_2}^{(i)}\Big(\rho_D^{(i)},\rho_r^{(i)}\Big)=\bar{Y}_{k_1,k_2}\Big(\rho_D^{(i)},\rho_r^{(i)}\Big)\\&-\breve{Y}_{k_1,k_2}\Big(\hat{F}_{D,c_i}^{(i)}\,,\hat{F}_{r,c_i}^{(i)};\hat{\mathbf{A}}^{(i-1)},\hat{\mathbf{F}}_D^{(i-1)},\hat{\mathbf{F}}_r^{(i-1)}\Big)\end{aligned}\tag{98}$$

with $k_1,k_2=0,1,2,3$; here, we have that (see (84) and (85))

$$\rho_D^{(i)}=\hat{F}_{D,c_i}^{(i)}/\bar{F}_D=\hat{l}^{(i)}-1/(2\bar{F}_D),\tag{99}$$

$$\rho_r^{(i)}=\hat{F}_{r,c_i}^{(i)}/\bar{F}_r=\hat{p}^{(i)}\tag{100}$$

and

$$\begin{aligned}&\breve{Y}_{k_1,k_2}\Big(\hat{F}_{D,c_i}^{(i)}\,,\hat{F}_{r,c_i}^{(i)};\hat{\mathbf{A}}^{(i-1)},\hat{\mathbf{F}}_D^{(i-1)},\hat{\mathbf{F}}_r^{(i-1)}\Big)\\&\triangleq\sum_{k=0}^{i-1}\bar{Y}_{k_1,k_2}\Big(\hat{F}_{D,c_i}^{(i)}\,,\hat{F}_{r,c_i}^{(i)};\hat{A}_k^{(i-1)},\hat{F}_{D_k}^{(i-1)},\hat{F}_{r_k}^{(i-1)}\Big)\end{aligned}\tag{101}$$

is the contribution given to $\bar{Y}_{k_1,k_2}^{(i)}(\rho_D^{(i)},\rho_r^{(i)})$ by all the estimated tones (in particular, $\bar{Y}_{k_1,k_2}(\hat{F}_{D,c_i}^{(i)}\,,\hat{F}_{r,c_i}^{(i)};\hat{A}_k^{(i-1)},\hat{F}_{D_k}^{(i-1)},\hat{F}_{r_k}^{(i-1)})$ represents the leakage due to the k-th estimated tone for $(F_D\,,F_r)=(\hat{F}_{D,c_i}^{(i)}\,,\hat{F}_{r,c_i}^{(i)})$).

e) The coefficients $\{a_\Omega\,,b_\Omega\,,c_\Omega\}$ ($\{a_\Delta\,,b_\Delta\,,c_\Delta\}$) on the basis of (71)-(73) ((76)-(78)) with $(\rho_D,\rho_r)=(\rho_D^{(i)},\rho_r^{(i)})$ and the initial estimate of the residual $\hat{\Omega}_i^{(0)}(\hat{\Delta}_i^{(0)})$ of Ω (Δ) on the basis of (69) or (74) with $X=\Omega$ ($X=\Delta$);

e) The initial fine estimate of the normalized Doppler frequency

$$\hat{F}_{D_i}^{(0)}=\hat{F}_{D,c_i}^{(0)}+\frac{\hat{\Omega}_i^{(0)}}{2\pi}\tag{102}$$

and that of the normalized delay

$$\hat{F}_{r_i}^{(0)}=\hat{F}_{r,c_i}^{(0)}+\frac{\hat{\Delta}_i^{(0)}}{2\pi}\tag{103}$$

on the basis of (42) and (43), respectively. The evaluation of $\hat{F}_D^{(0)}$ and $\hat{F}_r^{(0)}$ concludes the first step.

CSFDEC-S2 (*refinement of the last tone*) - In this step, $N_{\rm it}$ iterations are executed to refine the estimate of the parameters of the new tone detected in the previous step. The processing accomplished in this step follows closely that described in the refinement part (i.e., in the second step) of the CSFDE. For this reason, in each iteration, a new estimate of the complex amplitude and of the two residuals of the i-th tone are computed. This requires reusing (96)-(97) and (98)-(101) for the removal of spectral leakage. At the end of the last iteration, the estimates $(\check{F}_{D_i}^{(i)},\,\check{F}_{r_i}^{(i)},\check{A}_i^{(i)})$ of $(F_{D_i},\,F_{r_i},A_i)$ are available; these represent $(\hat{F}_{D_i}^{(i)},\,\hat{F}_{r_i}^{(i)},\hat{A}_i^{(i)})$ if the next step is not accomplished (i.e. if tone re-estimation is avoided).

CSFDEC-S3 (*tone re-estimation*) - This step is fed by the $(i+1)$ normalized delays $\{\hat{F}_{r_0}^{(i-1)},\,\hat{F}_{r_1}^{(i-1)},\,\ldots,\,\hat{F}_{r_{i-1}}^{(i-1)},\,\check{F}_{r_i}^{(i)}\}$, normalized Doppler frequencies $\{\hat{F}_{D_0}^{(i-1)},\,\hat{F}_{D_1}^{(i-1)},\,\ldots,\,\hat{F}_{D_{i-1}}^{(i-1)},\,\check{F}_{r_i}^{(i)}\}$ and the associated complex amplitudes $\{\hat{A}_0^{(i-1)},\,\hat{A}_1^{(i-1)},\,\ldots,\,\hat{A}_{i-1}^{(i-1)},\,\check{A}_i^{(i)}\}$. It consists in repeating the previous step for each of the detected tones, starting from the first tone and ending with the last (i.e., with the $(i+1)$-th) one. This means that, when re-estimating the k-th tone, the leakage due to all the other $(i-1)$ tones is removed (with $k=0,1,\ldots,i$). This allows to progressively refine the amplitude, normalised Doppler frequency and normalised delay of each tone, so generating the final estimates. Note that, in principle, this re-estimation procedure can be repeated multiple (say, $N_{\rm REF}$) times.

C. Computational complexity of the proposed algorithms

The computational complexity, in terms of number of *floating point operations* (flops), can be assessed for both the CSFDE and the CSFDEC algorithms as follows[8]. First of all, the overall computational cost of the CSFDE is expressed as

$$\mathcal{C}_{\mathrm{CSFDE}} = \mathcal{C}_0(\mathrm{CSFDE}) + N_{\mathrm{it}}\, \mathcal{C}_i(\mathrm{CSFDE}), \tag{104}$$

where $\mathcal{C}_0(\mathrm{CSFDE})$ and $\mathcal{C}_i(\mathrm{CSFDE})$ represent the computational cost of its initialization and that of each of its iterations, respectively. The cost $\mathcal{C}_0(\mathrm{CSFDE})$ is evaluated as[9]

$$\mathcal{C}_0(\mathrm{CSFDE}) = \mathcal{C}_{\hat{l},\hat{p}} + \mathcal{C}_{\bar{\mathbf{Y}}_{k_1,k_2}} + \mathcal{C}_{\hat{\Omega}} + \mathcal{C}_{\hat{\Delta}}, \tag{105}$$

where: a) $\mathcal{C}_{\hat{l},\hat{p}}$ is the contribution due to the computation of the couple $(\hat{l},\hat{p})$ on the basis of (81); b) $\mathcal{C}_{\bar{\mathbf{Y}}_{k_1,k_2}}$ is the contribution due to the computation of the matrices $\{\bar{\mathbf{Y}}_{k_1,k_2}\}$ on the basis of (66), including the evaluation of the spectrum $\bar{\mathbf{Y}}_{0,0}$; c) $\mathcal{C}_{\hat{\Omega}}$ and $\mathcal{C}_{\hat{\Delta}}$ are the contributions due to the evaluation of the estimates $\hat{\Omega}$ and $\hat{\Delta}$, respectively, on the basis of the quadratic equation (69). The cost $\mathcal{C}_{i,\mathrm{CSFDE}}$, instead, is evaluated as

$$\mathcal{C}_i(\mathrm{CSFDE}) \triangleq \mathcal{C}_{\bar{Y}} + \mathcal{C}_{\hat{\rho}_D} + \mathcal{C}_{\hat{\rho}_r} + \mathcal{C}_{\hat{A}} + \mathcal{C}_{\bar{Y}_{k_1,k_2}} + \mathcal{C}_{\hat{\Omega}} + \mathcal{C}_{\hat{\Delta}}, \tag{106}$$

where: a) $\mathcal{C}_{\bar{Y}}$ is the contribution due to the computation of $\bar{Y}(\hat{F}_D,\hat{F}_r)$ on the basis of (41) or of the interpolation of a few adjacent elements of $\bar{\mathbf{Y}}_s$ (54); b) $\mathcal{C}_{\hat{\rho}_D}$ ($\mathcal{C}_{\hat{\rho}_r}$) is the contributions due to the evaluation of $\hat{\rho}_D$ ($\hat{\rho}_r$) on the basis of (84) ((85)); c) $\mathcal{C}_{\hat{A}}$ is the contribution due to the evaluation of $\hat{A}$ on the basis of (53); d) $\mathcal{C}_{\bar{Y}_{k_1,k_2}}$ is the contribution due to the computation of the quantity $\bar{Y}_{k_1,k_2}(\hat{\rho}_D^{(i-1)},\hat{\rho}_r^{(i-1)})$ (98) through the interpolation of a few adjacent elements of the matrix $L_D\, L_r\, \bar{\mathbf{Y}}_{k_1,k_2}$ (see (66)) for the considered values of (k_1,k_2); e) $\mathcal{C}_{\hat{\Omega}}$ and $\mathcal{C}_{\hat{\Delta}}$ are the contributions due to the computation of $\hat{\Omega}$ and $\hat{\Delta}$ on the basis of (69). Based on the results illustrated in Appendix C, it can be proved that $\mathcal{C}_{\mathrm{CSFDE}} = \mathcal{O}(N_{\mathrm{CSFDE}})$, where

$$N_{\mathrm{CSFDE}} = 16\, M_0\, N_0 \log_2(M_0\, N_0) + N_{\mathrm{it}}\, 16\, I_D\, I_r, \tag{107}$$

and I_D (I_r) is the interpolation order adopted in the Doppler (range) domain for the evaluation of $\bar{Y}_{k_1,k_2}(\hat{\rho}_D^{(i-1)},\hat{\rho}_r^{(i-1)})$ (98). Note that, for small values of I_D and I_r (e.g., if a 2D linear or barycentric interpolation is used; see [38]), the contribution of the second term of the RHS of the last equation can be neglected, so that the order of the whole computational cost is well approximated by its first term, i.e. by the term originating from DSFT processing.

Our assessment of the complexity of the CSFDEC algorithm is based on the considerations illustrated in [40] for its 1D counterpart. This leads to concluding that $\mathcal{C}_{\mathrm{CSFDEC}} = \mathcal{O}(N_{\mathrm{CSFDEC}})$, where

$$N_{\mathrm{CSFDEC}} = 16\, M_0\, N_0 \log_2(M_0\, N_0) + K\, N_{\mathrm{it}}\; 16\, I_D\, I_r. \tag{108}$$

The last result holds if *tone re-estimation* is not accomplished. The first term appearing in the RHS of the last equation accounts for the initialization (and, in particular, for the computation of the matrices $\bar{\mathbf{Y}}_{0,0}$ (46) and $\left\{\bar{\mathbf{Y}}_{k_1,k_2};(k_1,k_2)\neq(0,0)\right\}$ (66)), whereas the second one for the fact that, in the CSFDEC algorithm, the CSFDE is executed K times. Note that the computational cost related to the estimation of the 2D-tones detected after the first one and to their frequency domain cancellation does not play an important role in this case. However, if *tone re-estimation* is executed in the CSFDEC algorithm, the parameter K appearing in the RHS of (108) is replaced by K^2, since this task involves all the estimated 2D-tones.

IV. Other Detection and Estimation Algorithms

In this subsection, various algorithms for the detection and estimation of multiple targets in an OFDM-based radar systems are briefly described, and their computational complexity is analysed. These algorithms are divided in FFT-based techniques, subspace-based methods and ML-based techniques.

A. FFT-based techniques

This class of algorithms includes the 2D periodogram method and the CLEAN algorithm [41], [42]. It is worth mentioning that the family of FFT-based techniques also includes the estimation algorithms derived in [43] and [44] for the estimation of multiple 2D complex tones. These last two algorithms differ from the CSFDEC in the fine estimation procedure, since a linear interpolation of the 2D spectrum and its parabolic fitting are employed in [43] and [44], respectively. Moreover, their computational complexity is limited, being slightly larger than that of the 2D periodogram method. However, our computer simulations have evidenced that the accuracy they achieve in presence of closely spaced targets is quite poor. For this reason, they are not taken into consideration in the following.

[8]The general criteria adopted in our evaluation of computational costs are summarised in [39, App. C].

[9]Note that the evaluation of the estimate of the tone complex amplitude is neglected, being based on (53), that requires a negligible computational effort.

1) Two-dimensional periodogram method: This method requires the computation of the so-called *range-Doppler* map [17], i.e. of the quantity

$$J(l,p) = |S(l,p)|^2, \tag{109}$$

with $l = 0, 1, ..., M_0 - 1$ and $p = 0, 1, ..., N_0 - 1$; here,

$$S(l,p) \triangleq \frac{1}{M_0 N_0} \sum_{m=0}^{M-1} \sum_{n=0}^{N-1} \hat{H}_{m,n} \left(M_{m,n}(F_D[l], F_r[p])\right)^*, \tag{110}$$

is the coefficient (l,p) of the order (M_0, N_0) DSFT of the 2D sequence $\{\hat{H}_{m,n}\}$,

$$F_D[l] = l/M_0 - 1/2 \tag{111}$$

and

$$F_r[p] = p/N_0. \tag{112}$$

In the case of a single target, the estimates of its normalized Doppler frequency F_D and normalized delay F_r are evaluated as $\hat{F}_D = F_D[\hat{l}]$ and $\hat{F}_r = F_r[\hat{p}]$, respectively, where

$$\left(\hat{l}, \hat{p}\right) \triangleq \max_{\tilde{l} \in \mathcal{S}_{M_0}, \tilde{p} \in \mathcal{S}_{N_0}} J\left(\tilde{l}, \tilde{p}\right). \tag{113}$$

Moreover, the target complex amplitude A is estimated as

$$\hat{A} = L_D \, L_r \, S\left(\hat{l}, \hat{p}\right). \tag{114}$$

with $L_D = M_0/M$ and $L_r = N_0/N$ (see (49) and (50), respectively). A similar procedure is followed in a multi-target scenario. In fact, in that case, multiple local maxima[10] should be expected in the *range-Doppler* map, and the parameters of the target associated with each of them can be estimated through (111), (112) and (114).

The most computationally intensive task required by this method is represented the evaluation of the above mentioned order (M_0, N_0) order DSFT (see (110)). For this reason, its computational cost is $\mathcal{C}_{\rm PM} = \mathcal{O}(N_{\rm PM})$, where

$$N_{\rm PM} = M_0 \, N_0 \, \log_2(M_0 \, N_0). \tag{115}$$

2) CLEAN algorithm: The adoption of the CLEAN algorithm in radar systems has been proposed in [41] and [42], where, however, its use in *stepped frequency continuous wave* (SFCW) radar technology has been investigated. In this paragraph, we show how this algorithm can be also employed for jointly estimating the range and velocity of multiple targets in OFDM-based radar systems.

The CLEAN algorithm exploits the same cost function as the 2D periodogram method (see (109)), but, unlike it, employs an iterative target cancellation process. This means that, within each of its iterations, a new target is detected, its parameters are estimated and its contribution to the above mentioned cost function is cancelled; this results in a residual cost function, which is passed to the next iteration.

The processing executed by the CLEAN algorithm consists in an initialization step followed by an iterative procedure. In the initialization, we set the iteration index k to 0 and

$$\hat{H}_{m,n}[0] = \hat{H}_{m,n}, \tag{116}$$

with $m = 0, 1, ..., M - 1$ and $n = 0, 1, ..., N - 1$. Then, in the k-th iteration (with $k = 0, 1, ..., \hat{K} - 1$, where $\hat{K}$ denotes the overall number of detected targets), the four steps described below are carried out sequentially.

1) *Computation of the cost function* - The cost function (see (109))

$$J_k(l,p) = |S_k(l,p)|^2 \tag{117}$$

is evaluated for $l = 0, 1, ..., M_0 - 1$ and $p = 0, 1, ..., N_0 - 1$; here, $S_k(l,p)$ is expressed by (110), where, however, $\hat{H}_{m,n}$ is replaced by $\hat{H}_{m,n}[k]$.

2) *Estimation of the parameters of a new target* - A search for the global maximum over the set $\{J_k(l,p);\ l \in \mathcal{S}_{M_0},\ p \in \mathcal{S}_{N_0}\}$ (collecting $M_0 \cdot N_0$ values) is performed to detect a new target (i.e., the k-th target); the value of the couple (l,p) associated with the global maximum is denoted $(\hat{l}_k, \hat{p}_k)$. Then, the estimates of the normalised frequency $\hat{F}_{D_k}$ and the normalised delay $\hat{F}_{r_k}$ of the k-th target are evaluated as $F_D[\hat{l}_k]$ and $F_r[\hat{p}_k]$ (see (111) and (112)), respectively, whereas that of its complex amplitude $\hat{A}_k$ is evaluated according to (114), where $S(\hat{l}, \hat{p})$ is replaced by $S_k(\hat{l}_k, \hat{p}_k)$.

3) *Threshold test for the detection of false targets* - If

$$\left|\hat{A}_k\right| < T_{\rm CLEAN}, \tag{118}$$

[10]In our computer simulations, the *Fast* 2D *peak finder* function available in MatlabR2022a has been exploited to locate all the relevant peaks in the range-Doppler map.

where T_{CLEAN} denotes a proper (positive) threshold, a false target is detected and the execution is stopped by moving to step 5); otherwise, we proceed with the next step.

4) *Cancellation of the last detected target* - The new residual frequency response

$$\hat{H}_{m,n}[k+1] \triangleq \hat{H}_{m,n}[k] - \hat{A}_k \, M_{m,n}\Big(\hat{F}_{D_k}, \hat{F}_{r_k}\Big) \tag{119}$$

is evaluated to cancel the contribution of the last detected target to $\hat{H}_{m,n}[k]$ (with $m = 0, 1, ..., M-1$ and $n = 0, 1, ..., N-1$); note that the function $M_{m,n}(\cdot, \cdot)$ is defined by (25). Then, the iteration index k is increased by one and a new iteration is started (i.e., we go back to step 1));

5) *End* - The final output provided by the CLEAN algorithm is represented by the set $\{(\hat{F}_{D_k}, \hat{F}_{r_k}, \hat{A}_k); k = 0, 1, ..., \hat{K}-1\}$, where $\hat{K}$ represents the last value taken on by the iteration index k.

The serial cancellation procedure expressed by eq. (119) may suffer from *error accumulation*; this is due to the fact that the effects of errors in the estimation of target parameters accumulate over successive iterations. This may result in: a) poor accuracy in the presence of multiple and/or closely spaced targets; b) the detection of false targets. These considerations motivate the use of a *refinement procedure* to be executed after the last iteration of the CLEAN algorithm. This procedure consists of N_{REF} iterations. In its i-th iteration (with $i = 1, 2, ..., N_{\mathrm{REF}}$), the refined estimates $\{(\hat{F}_{D_k}^{(i)}, \hat{F}_{r_k}^{(i)}, \hat{A}_k^{(i)}); k = 0, 1, ..., \hat{K}-1\}$ of the parameters of the $\hat{K}$ targets detected by the CLEAN algorithm are computed. To this aim, we first compute $(\hat{l}_k^{(i)}, \hat{p}_k^{(i)})$, that represents the value of the couple (l, p) maximising the function

$$J_k^{(i)}(l, p) = |S_k^{(i)}(l, p)|^2. \tag{120}$$

over a specific grid, whose center depends on both $\hat{F}_{D_k}^{(i-1)}$ and $\hat{F}_{r_k}^{(i-1)}$, and whose step size gets smaller as i increases. Here, $S_k^{(i)}(l, p)$ is still evaluated on the basis of (110), but the quantity $\hat{H}_{m,n}$ appearing in the RHS of that equation is replaced by

$$\hat{H}_{m,n}^{(i)}[k] = \hat{H}_{m,n}[0] - \sum_{j=0,\, j\neq k}^{\hat{K}-1} \hat{A}_j^{(i-1)} \, M_{m,n}\Big(\hat{F}_{D_j}^{(i-1)}, \hat{F}_{r_j}^{(i-1)}\Big) \tag{121}$$

for $k = 0, 1, ..., \hat{K}-1$. Moreover, the search grid for $F_{X_k}^{(i)}$ (with $X = r$ and D) is selected after establishing which of the following couple of inequalities is satisfied: 1) $F_{X,\min} \leqslant \hat{F}_{X_k}^{(i-1)} < F_{X,\min} + \delta_X$; 2) $F_{X,\min} + \delta_X \leqslant \hat{F}_{X_k}^{(i-1)} \leqslant F_{X,\max} - \delta_X$; 3) $F_{X,\max} - \delta_X < \hat{F}_{X_k}^{(i-1)} \leqslant F_{X,\max}$; here, $\delta_X = 1/M_0$ ($\delta_X = 1/N_0$) for $X = D$ ($X = r$). In fact, the z-th tentative value $\tilde{F}_{X_k}^{(i)}[z]$ for $F_{X_k}^{(i)}$ in the search for the maximum of $J_k^{(i)}(l, p)$ (120) is evaluated as $F_{X,\min} + \Delta_X[i]\, z\, \delta_X$, $\hat{F}_{X_k}^{(i-1)} + \Delta_X[i](z\, \delta_X - 1/2)$ and $F_{X,\max} + \Delta_X[i](z\, \delta_X - 1)$, in cases 1), 2) and 3), respectively; here, $\Delta_X[i] \triangleq \delta_X / i$, $z = l$ ($z = p$) if $X = D$ ($X = r$) $l = 0, 1, ..., \tilde{M}_0 - 1$ ($p = 0, 1, ..., \tilde{N}_0 - 1$), with $\tilde{M}_0$ ($\tilde{N}_0$) being the number of searching points for normalized Doppler frequency (normalized delay). Then, the estimates of $\hat{F}_{D_k}^{(i)} = F_D[\hat{l}_k^{(i)}]$ and $\hat{F}_{r_k}^{(i)} = F_r[\hat{p}_k^{(i)}]$ of F_{D_k} and F_{r_k}, respectively, are evaluated (see (111) and (112), respectively). Finally, the amplitude $\hat{A}_k^{(i)}$ is computed on the basis of (114), where, however, $S(\hat{l}, \hat{p})$ is replaced by $S_k^{(i)}(\hat{l}_k^{(i)}, \hat{p}_k^{(i)})$.

It is important to point out that: a) the evaluation of $\hat{H}_{m,n}^{(i)}[k]$ according to (121) aims at cancelling the contribution given to $\hat{H}_{m,n}[0]$ by the $(\hat{K}-1)$ targets different from the k-th one in the i-th iteration; b) at the end of the last (i.e., the N_{REF}-th) iteration, the refined estimates $\{(\hat{F}_{D_k}^{(N_{\mathrm{REF}})}, \hat{F}_{r_k}^{(N_{\mathrm{REF}})}, \hat{A}_k^{(N_{\mathrm{REF}})}); k = 0, 1, ..., \hat{K}-1\}$ become available.

It can be shown that the computational cost of the CLEAN algorithm with refinement is $\mathcal{O}(N_{\mathrm{CL}})$, where (see [41, Sec. III-E, eq. (43)])

$$N_{\mathrm{CL}} = \bar{N}_{\mathrm{CL}}(M_0, N_0) + N_{\mathrm{REF}} \, \bar{N}_{\mathrm{CL}}\big(\tilde{M}_0, \tilde{N}_0\big). \tag{122}$$

Here,

$$\bar{N}_{\mathrm{CL}}(M_0, N_0) = MN(6M_0N_0 + 15) + 2M_0N_0(M + N) \tag{123}$$

is the contribution due a single iteration of the algorithm; note that the parameters (M_0, N_0) $((\tilde{M}_0, \tilde{N}_0))$ define the grid size for the initialization (for the refinement) step.

B. Subspace-based methods

This class of methods includes the 2D-MUSIC algorithm and the 2D-ESPRIT. However, in the following we focus on the first algorithm only since the latter performs similarly as 2D-MUSIC and does not require a lower computational complexity [31], [45].

1) Two-dimensional MUSIC algorithm: The use of the 2D-MUSIC algorithm in OFDM-based radar systems has been investigated in [27], [28] and [46]. This algorithm requires a prior estimate (denoted $\hat{K}$) of K and consists of the following steps. First, the columns of the $M \times N$ matrix $\hat{\mathbf{H}}_{0,0} = [\hat{H}_{m,n}]$ (see (48)) are stacked to form the $(M\,N)$-dimensional vector $\bar{\mathbf{H}}$; based on this, the $(M\,N) \times (M\,N)$ correlation matrix

$$\mathbf{R} \triangleq \frac{1}{MN} \bar{\mathbf{H}}\, \bar{\mathbf{H}}^H \tag{124}$$

is computed. Then, the *pseudo-spectrum*

$$P_{\mathrm{MUSIC}}[l,p] \triangleq \frac{1}{\left\| \mathbf{Q}_n^H\, \bar{\mathbf{M}}[l,p] \right\|^2} \tag{125}$$

is evaluated for $l = 0, 1, \ldots, M_0 - 1$ and $p = 0, 1, \ldots, N_0 - 1$; here, M_0 and N_0 are integer parameters defining the size of the search space for the normalized Doppler frequency and normalized delay, respectively, $\bar{\mathbf{M}}[l,p]$ is a $(MN) \times (M_0\, N_0)$ matrix whose (m,n)-th element is defined by (25) (with F_D and F_r expressed by (111) and (112), respectively) and $\mathbf{Q}_n$ is $(MN) \times (MN - \hat{K})$ matrix, whose columns represent the $(MN - \hat{K})$ eigenvectors of $\mathbf{R}$ (124) associated with noise.

Given the pseudo-spectrum (125), the estimates of the normalized delay and the normalized Doppler frequency are evaluated by finding its global maximum (the $\hat{K}$ highest local peaks) in the case of a single target (multiple targets).

The overall 2D-MUSIC complexity is $\mathcal{O}(N_{\mathrm{MUSIC}})$, where

$$N_{\mathrm{MUSIC}} = C_{\mathrm{R}} + C_{\mathrm{e}} + C_{\mathrm{P}}. \tag{126}$$

Here, we have that: a) $C_{\mathrm{R}} = 10(MN)^2 + 2MN - 2$ is the cost due to the computation of the covariance matrix $\mathbf{R}$ (see (124)); b) $C_{\mathrm{e}} \approx (MN)^3$ is the contribution due to computation of the eigenvalues of the matrix $\mathbf{R}$; c) $C_{\mathrm{P}} = M_0\, N_0 \big(8(M\,N)^2 + M\,N\big)$ is the contribution due to the evaluation of the pseudo-spectrum (see (125)).

C. Maximum likelihood-based techniques

This class of algorithms includes: a) the approximate ML method recently proposed in [31]; b) the MWL algorithm developed in [41] and [42] for joint range and azimuth estimation of multiple targets in FMCW radars; c) the *expectation maximization* (EM) algorithm. As far as point a) is concerned, it is important to point out that, in our work, the ML algorithm devised in [31] has been properly modified to adapt it to our signal model (30), since *inter-pulse* and *inter-subcarrier* Doppler effects are ignored; the resulting algorithm, called *modified alternating projection* ML (MAP-ML) exploits alternating projections to turn a 2D optimization problem in a couple of simpler 1D problems. Moreover, another algorithm, called *modified Zhang* ML (MZML), has been also investigated for completeness; it uses the same metric as the MAP-ML algorithm, but requires solving a 2D optimization problem. Note that both the MAP-ML and MZML algorithms require a prior estimate (denoted $\hat{K}$) of K.

1) Modified Zhang maximum likelihood algorithm: The processing accomplished by this algorithm is iterative; in each iteration, the estimates of the detected targets are refined. The algorithm is initialised by setting the iteration index i to 1 and selecting the initial estimates $\hat{F}_{D_k}^{(0)}$ and $\hat{F}_{r_k}^{(0)}$ of the normalized Doppler frequency F_{D_k} and normalized delay F_{r_k}, respectively, with $k = 0, 1, ..., \hat{K} - 1$ according to (111) and (112); here, the couple $(\hat{l}_k^{(0)}, \hat{p}_k^{(0)})$ is computed on the basis of (113).

Then, the iterations are started. The i-th iteration (with $i = 1, ..., N_{\mathrm{REF}}$, where N_{REF} denotes the overall number of iterations) is fed by the vectors

$$\hat{\mathbf{F}}_D^{(i-1)} = \left[\hat{F}_{D_0}^{(i-1)}, \hat{F}_{D_1}^{(i-1)}, \ldots, \hat{F}_{D_{\hat{K}-1}}^{(i-1)} \right]^T \tag{127}$$

and

$$\hat{\mathbf{F}}_r^{(i-1)} = \left[\hat{F}_{r_0}^{(i-1)}, \hat{F}_{r_1}^{(i-1)}, \ldots, \hat{F}_{r_{\hat{K}-1}}^{(i-1)} \right]^T, \tag{128}$$

collecting the estimates of the normalised Doppler frequency and normalised delay, respectively, of the $\hat{K}$ tones estimated in the previous $(i-1)$ iterations, and produces the new estimates $\hat{\mathbf{F}}_D^{(i)}$ and $\hat{\mathbf{F}}_r^{(i)}$. Moreover, it consists of two steps, that are repeated sequentially for each target (i.e., for $k = 0, 1, \ldots, \hat{K} - 1$); their description is provided below for the k-th target.

1) *Computation of the cost function* - In this step, the cost function

$$J_k^{(i)}[l,p] \triangleq \bar{\mathbf{H}}^H\, \mathbf{P}_k^{(i)}(l,p)\, \bar{\mathbf{H}} \tag{129}$$

is evaluated for $l = 0, 1, ..., M_0 - 1$ and $p = 0, 1, ..., N_0 - 1$, with M_0 (N_0) being the size of the search space for the normalised Doppler frequency (normalised delay); here, $\bar{\mathbf{H}}$ is the $(M\,N)$-dimensional vector resulting from the ordered concatenation of the columns of the $M \times N$ matrix $\hat{\mathbf{H}}_{0,0}$ (48),

$$\mathbf{P}_k^{(i)}(l,p) \triangleq \breve{\mathbf{M}}_k^{(i)} \left(\left(\breve{\mathbf{M}}_k^{(i)} \right)^H \breve{\mathbf{M}}_k^{(i)} \right)^{-1} \left(\breve{\mathbf{M}}_k^{(i)} \right)^H \tag{130}$$

is an $(MN) \times (MN)$ *orthogonal projection matrix*[11], $\breve{\mathbf{M}}_k^{(i)} = \breve{\mathbf{M}}_k^{(i)}(\tilde{F}_{D_k}^{(i)}[l], \tilde{F}_{r_k}^{(i)}[p])$ is an $(M\,N) \times \hat{K}$ matrix defined as

$$\breve{\mathbf{M}}_k^{(i)} \triangleq \Big[\mathbf{M}_0^{(i-1)}, \mathbf{M}_1^{(i-1)}, ..., \mathbf{M}_{k-1}^{(i-1)}, \mathbf{M}_{k+1}^{(i-1)}, \\ ..., \mathbf{M}_{\hat{K}-1}^{(i-1)}, \mathbf{M}^{(i)}\Big]; \tag{131}$$

moreover, $\tilde{F}_{D_k}^{(i)}[l]$ and $\tilde{F}_{r_k}^{(i)}[p]$ are tentative values of F_{D_k} and F_{r_k}, respectively (these are evaluated on the basis of the procedure described for $\tilde{F}_{X_k}^{(i)}[z]$, with $X = D$ and r, right after (121)) and $\mathbf{M}_u^{(i-1)}$ ($\mathbf{M}^{(i)}$) is an $(M\,N)$-dimensional column vector resulting from the ordered concatenation of the columns of the $M \times N$ matrix $\hat{\mathbf{M}}_u^{(i-1)} \triangleq [M_{m,n}(\hat{F}_{D_u}^{(i-1)}, \hat{F}_{r_u}^{(i-1)})]$ ($\hat{\mathbf{M}}^{(i)} = \hat{\mathbf{M}}^{(i)}(\tilde{F}_{D_k}^{(i)}[l], \tilde{F}_{r_k}^{(i)}[p]) \triangleq [M_{m,n}(\tilde{F}_{D_k}^{(i)}[l], \tilde{F}_{r_k}^{(i)}[p])]$; with $m = 0, 1, \ldots, M-1$ and $n = 0, 1, \ldots, N-1$).

It is worth noting that: a) the vector $\mathbf{M}_u^{(i-1)}$ represents the contribution (evaluated on the basis of the parameters estimated in the $(i-1)$-th iteration) of the u-th target (with $u \neq k$) to the vector $\mathbf{M}^{(i)}(\tilde{F}_{D_k}^{(i)}[l], \tilde{F}_{r_k}^{(i)}[p])$ computed for the k-th target in the i-th iteration; b) building the matrix $\breve{\mathbf{M}}_k^{(i)}$ according to (131) allows to compensate for the *leakage* effect in the evaluation of the projection matrix $\mathbf{P}_k^{(i)}[l, p]$ (130).

2) *Target detection and estimation* - In this step, the estimates $(\hat{F}_{D_k}^{(i)}, \hat{F}_{r_k}^{(i)})$ of (F_{D_k}, F_{r_k}) are computed on the basis of (111) and (112); here,

$$\Big(\hat{l}_k^{(i)}, \hat{p}_k^{(i)}\Big) = \arg \max_{\tilde{l} \in \mathcal{S}_{M_0}, \tilde{p} \in \mathcal{S}_{N_0}} \Big|J_k^{(i)}\Big(\tilde{l}, \tilde{p}\Big)\Big|. \tag{132}$$

Then, the new estimate $\hat{A}_k^{(i)}$ of the complex amplitude A_k is evaluated as

$$\hat{A}_k^{(i)} = \left(\left(\breve{\mathbf{M}}_k^{(i)}\left(\hat{F}_{D_k}^{(i)}, \hat{F}_{r_k}^{(i)}\right)\right)^H \breve{\mathbf{M}}_k^{(i)}\left(\hat{F}_{D_k}^{(i)}, \hat{F}_{r_k}^{(i)}\right)\right)^{-1} \\ \cdot\left(\breve{\mathbf{M}}_k^{(i)}\left(\hat{F}_{D_k}^{(i)}, \hat{F}_{r_k}^{(i)}\right)\right)^H \tag{133}$$

At the end of the last iteration, the vectors $\hat{\mathbf{F}}_D^{(N_{\rm REF})}$, $\hat{\mathbf{F}}_r^{(N_{\rm REF})}$ and $\hat{\mathbf{A}}^{(N_{\rm REF})}$, collecting the normalised frequencies, the normalized delays and the complex amplitudes of the $\hat{K}$ targets are available.

The overall computational cost of MZML algorithm can be expressed as

$$\mathcal{C}_{\rm MZML} \triangleq \mathcal{C}_{0,\rm MZML} + N_{\rm REF}\,\mathcal{C}_{i,\rm MZML}, \tag{134}$$

where $\mathcal{C}_{0,\rm MZML}$ is the cost of its initialization (i.e., the same cost as the periodogram method; see (115)), whereas

$$\mathcal{C}_{i,\rm MZML} \triangleq \mathcal{C}_P + \mathcal{C}_J + \mathcal{C}_{l,p} \tag{135}$$

represents the cost of a single iteration; here, we have that: a) $\mathcal{C}_P \approx 8M_0\,N_0\,\hat{K}^2M^2N^2$ is the cost due to the evaluation of the $M_0\,N_0$ projection matrices $\{\mathbf{P}_k^{(i)}[l, p]\}$ (see (130)) for all the $\hat{K}$ targets; b) $\mathcal{C}_J \approx 8M_0\,N_0\,\hat{K}\,M^2N^2$ is the cost due to the evaluation of the $M_0\,N_0$ cost functions $\{J_k^{(i)}[l, p]\}$ (see (129)); c) $\mathcal{C}_{l,p} = 4M_0\,N_0\,\hat{K}$ is the cost due to solving optimization problem in (132). Based on these results, it can be shown that the computational cost of MZML algorithm is $\mathcal{O}(N_{\rm MZML})$, where

$$N_{\rm MZML} = N_{\rm REF}\,8\,M_0\,N_0\Big(\hat{K}^2 + \hat{K}\Big)M^2N^2 \tag{136}$$

2) Modified alternating projection maximum likelihood algorithm: Similarly as the MZML algorithm, the MAP-ML algorithm exploits the cost function $J_k^{(i)}(l, p)$ (129) in the estimation of the parameters of the k-th target and it is initialised exactly in the same way; however, an *alternating projection* (AP) is exploited for its maximization in order to replace the 2D optimization problem (132) with two 1D optimization problems. In practice, in its i-th iteration, the couple $(\hat{l}_k^{(i)}, \hat{p}_k^{(i)})$ appearing in the LHS of (132) is evaluated as follows. First we compute

$$\hat{p}_k^{(i)} = \arg \max_{\tilde{p} \in \mathcal{S}_{N_0}} \Big|J_k^{(i)}\Big(\hat{l}_k^{(i-1)}, \tilde{p}\Big)\Big|. \tag{137}$$

Then, we evaluate

$$\hat{l}_k^{(i)} = \arg \max_{\tilde{l} \in \mathcal{S}_{M_0}} \Big|J_k^{(i)}\Big(\tilde{l}, \hat{p}_k^{(i)}\Big)\Big| \tag{138}$$

Note that: a) the evaluation of $J_k^{(i)}(\hat{l}_k^{(i-1)}, \tilde{p})$ in (137) ($J_k^{(i)}(\tilde{l}, \hat{p}_k^{(i)})$ in (138)) requires the computation of matrix $\breve{\mathbf{M}}_k^{(i)}(\hat{F}_{D_k}^{(i-1)}, F_{r_k}^{(i)}[\tilde{p}])$ ($\breve{\mathbf{M}}_k^{(i)}(F_{D_k}^{(i)}[\tilde{l}], \hat{F}_{r_k}^{(i)})$) (131); b) if $i = 1$, $\hat{F}_{D_k}^{(0)}$ is evaluated on the basis of (111) with $\hat{l}_k^{(0)}$ computed on the basis of (113); c) the estimate of the complex amplitude is computed on the basis of (133).

[11]The dependence of $\breve{\mathbf{M}}_k^{(i)}$ on the trial couple $(\tilde{F}_{D_k}^{(i)}[l], \tilde{F}_{r_k}^{(i)}[p])$ is not explicitly shown in the definition (130) for simplicity.

The overall computational cost $\mathcal{C}_{\mathrm{MAP-ML}}$ of the MAP-ML algorithm can be expressed as

$$\mathcal{C}_{\mathrm{MAP-ML}} = \mathcal{C}_{0,\mathrm{MAP-ML}} + N_{\mathrm{REF}}\, \mathcal{C}_{i,\mathrm{MZAP}}, \tag{139}$$

where $\mathcal{C}_{0,\mathrm{MAP-ML}}$ is the contribution due to its initialization (this is the same as MZML algorithm), whereas

$$\mathcal{C}_{i,\mathrm{MAP-ML}} = \mathcal{C}_{P_r} + \mathcal{C}_{P_D} + \mathcal{C}_{J_r} + \mathcal{C}_{J_D} + \mathcal{C}_p + \mathcal{C}_l \tag{140}$$

is the contribution due to each of its iterations. Moreover, in the last formula, we have that: a) $\mathcal{C}_{P_r} \approx 8N_0\hat{K}^2M^2N^2$ ($\mathcal{C}_{P_D} \approx 8M_0\hat{K}^2M^2N^2$) and $\mathcal{C}_{J_r} \approx 8N_0\hat{K}M^2N^2$ ($\mathcal{C}_{J_D} \approx 8M_0\hat{K}M^2N^2$) are the costs due to the evaluation of the projection matrices $\{\mathbf{P}_k^{(i)}[l,p]\}$ (see (130)) and of the cost functions $\{J_k^{(i)}[l,p]\}$ (see (129)), respectively, in the first (second) 1D optimization; b) $\mathcal{C}_p = 4N_0$ ($\mathcal{C}_l = 4M_0$) is the cost required by solving the 1D maximization in (137) ((138)).

Based on (139)-(140), it can be shown that the computational cost of MAP-ML algorithm is $\mathcal{O}(N_{\mathrm{MAP-ML}})$, where

$$N_{\mathrm{MAP-ML}} = N_{\mathrm{REF}}\, 8(M_0+N_0)\,(\hat{K}^2+\hat{K})\,M^2N^2. \tag{141}$$

3) MWL algorithm: Similarly as the CLEAN algorithm, the MWL algorithm, in each of its iterations, estimates the parameters of a new target. However, unlike the CLEAN algorithm, the MWL algorithm requires solving 1D optimization problems only. Moreover, in [41] it has been shown that it can achieve similar and even better accuracy than the CLEAN algorithm with a smaller computational effort.

The processing accomplished by this algorithm evolves through the four steps described below.

1) *Coarse estimation of the Doppler of a new target* - In this step, the *coarse estimate* $\breve{F}_{D_k}$ of the Doppler frequency F_{D_k} of a new (namely, of the k-th) target is evaluated solving the 1D optimization problem

$$\breve{l}_k \triangleq \arg\max_{\tilde{l}\in\mathcal{S}_{M_0}} \mathbf{a}^H\Big(F_D\Big[\tilde{l}\Big]\Big)\mathbf{R}[k]\,\mathbf{a}\Big(F_D\Big[\tilde{l}\Big]\Big) \tag{142}$$

where $F_D[\tilde{l}]$ is defined by (111), $\mathbf{a}(F_D[\tilde{l}])$ is an M-dimensional column vector whose m-th element, denoted $a_m(F_D[\tilde{l}])$, is defined by (26) (with $m=0,1,\ldots,M-1$), $\mathbf{R}[k]=[R_{m,m'}[k]]$ is an $M\times M$ autocorrelation matrix such that

$$R_{m,m'}[k] \triangleq \frac{1}{N}\sum_{n=0}^{N-1}\hat{H}_{m,n}[k]\Big(\hat{H}_{m',n}[k]\Big)^H, \tag{143}$$

with $m=0,1,\ldots,M-1$ and $m'=0,1,\ldots,M-1$, and $\hat{H}_{m,n}[k]$ is evaluated on the basis of (119) for $n=0,1,\ldots,N-1$. Given $\breve{l}_k$ (142), the coarse estimate is computed as $\breve{F}_{D_k}=F_D[\breve{l}_k]$ (see (111)).

2) *Estimation of target delay* - In this step, an estimate $\hat{F}_{r_k}$ of the normalized delay F_{r_k} characterising the k-th target is evaluated by solving another 1D optimization problem. This requires:

a) Computing the N-dimensional column vector

$$\hat{\mathbf{v}}_k \triangleq [\hat{v}_k[0],\hat{v}_k[1],...,\hat{v}_k[N-1]]^T, \tag{144}$$

whose n-th element is defined as

$$\hat{v}_k[n] \triangleq \Big[\mathbf{a}^H\Big(\breve{F}_{D_k}\Big)\,\mathbf{a}\Big(\breve{F}_{D_k}\Big)\Big]^T\mathbf{a}^H\Big(\breve{F}_{D_k}\Big)\,\mathbf{H}_n[k] \tag{145}$$

with $n=0,1,\ldots,N-1$; here, $\mathbf{H}_n[k]\triangleq[\hat{H}_{0,n}[k],\,\hat{H}_{1,n}[k],\,\ldots,\,\hat{H}_{M-1,n}[k]]^T$ is an M-dimensional vector.

b) Evaluating

$$\hat{p}_k = \arg\max_{\tilde{p}\in\mathcal{S}_{N_0}}\big\|\mathbf{b}^H(F_r[\tilde{p}])\,\hat{\mathbf{v}}_k\big\|^2. \tag{146}$$

Here, $F_r[\tilde{p}]$ is defined by (112) and $\mathbf{b}(F_r[\tilde{p}])$ is an N-dimensional column vector whose n-element (with $n=0,1,\ldots,N-1$) is denoted $b_n(F_r[\tilde{p}])$ and defined by (27). Given $\hat{p}_k$ (146), the final estimate $\hat{F}_{r_k}$ of the target delay is evaluated according to (112) with $p=\hat{p}_k$.

3) *Fine estimation of target Doppler* - In this step, the fine estimate $\hat{F}_{D_k}$ of the normalised Doppler F_{D_k} characterising the k-th target is evaluated by solving the last 1D optimization problem. In fact, we compute

$$\hat{l}_k \triangleq \arg\max_{\tilde{l}\in\mathcal{S}_{M_0}}\Big|\mathbf{a}^H\Big(F_D\Big[\tilde{l}\Big]\Big)\hat{\mathbf{B}}\Big(\hat{F}_{r_k}\Big)\Big|^2, \tag{147}$$

where $\hat{\mathbf{B}}(\hat{F}_{r_k})$ is an M-dimensional row vector, whose m-th element is defined as

$$\hat{B}_m\Big(\hat{F}_{r_k}\Big) \triangleq \left[\sum_{n=0}^{N-1}\hat{H}_{m,n}\,b_n^*\Big(\hat{F}_{r_k}\Big)\right]\hat{C}^{-1}\Big(\hat{F}_{r_k}\Big); \tag{148}$$

here,

$$\hat{C}\Big(\hat{F}_{r_k}\Big) \triangleq \sum_{n=0}^{N-1} b_n\Big(\hat{F}_{r_k}\Big) b_n^*\Big(\hat{F}_{r_k}\Big). \tag{149}$$

Given $\hat{l}_k$ (147), $\hat{F}_{D_k}$ is computed according to (111) with $l = \hat{l}_k$.

4) *Estimation of target complex amplitude* - In this step, the estimate

$$\hat{A}_k = \Big\|\mathbf{a}\Big(\hat{F}_{D_k}\Big)\Big\|^{-2} \mathbf{a}^H\Big(\hat{F}_{D_k}\Big)\, \hat{\mathbf{B}}\Big(\hat{F}_{r_k}\Big), \tag{150}$$

of the complex amplitude A_k is evaluated.

Similarly as the CLEAN algorithm, at the end of the last step a false target is detected if

$$\big|\hat{A}_k\big| < T_{\mathrm{MWL}}, \tag{151}$$

where T_{MWL} denotes a proper (positive) threshold. When this occurs, the execution is stopped; otherwise, a new iteration is started going back to the first step.

An iterative procedure can be employed to refine the target estimates generated by the MWL algorithm. Similarly as the CLEAN algorithm, this refinement procedure is based on the idea of evaluating a new estimate of the parameters of each target after removing the spectral contribution of the other $\hat{K} - 1$ targets, i.e. their *leakage*. More specifically, in its i-th iteration (with $i = 1, 2, ..., N_{\mathrm{REF}}$), the refined estimates $\{(\hat{F}_{D_k}^{(i)},\, \hat{F}_{r_k}^{(i)},\, \hat{A}_k^{(i)});\ k = 0, 1, ..., \hat{K} - 1\}$ of the parameters of the $\hat{K}$ targets detected by the MWL algorithm are computed; here, $\hat{F}_{D_k}^{(i)}$ and $\hat{F}_{r_k}^{(i)}$ are computed according to (111) and (112) with $l = \hat{l}_k^{(i)}$ and $p = \hat{p}_k^{(i)}$. Such estimates are evaluated as follows. First, we compute the coarse estimate $\breve{F}_{D_k}^{(i)} = (\breve{l}_k^{(i)}/M_0 - 1/2)$ of F_{D_k}, where (see (142))

$$\breve{l}_k^{(i)} \triangleq \arg \max_{\tilde{l} \in \mathcal{S}_{M_0}} \mathbf{a}^H\Big(F_D\Big[\tilde{l}\Big]\Big) \mathbf{R}^{(i)}[k]\, \mathbf{a}\Big(F_D\Big[\tilde{l}\Big]\Big) \tag{152}$$

and $\mathbf{R}^{(i)}[k]$ is an $M \times M$ matrix whose element (m, m') is still defined by (143), where, however, $\hat{H}_{m,n}[k]$ is replaced by

$$\breve{H}_{m,n}^{(i)}[k] = \hat{H}_{m,n}[0] - \sum_{j=0,\, j\neq k}^{\hat{K}-1} \hat{A}_j^{(i-1)}\, M_{m,n}\Big(\hat{F}_{D_j}^{(i-1)}, \hat{F}_{r_j}^{(i-1)}\Big). \tag{153}$$

Then, we evaluate

$$\hat{p}_k^{(i)} = \arg \max_{\tilde{p} \in \mathcal{S}_{N_0}} \Big\|\mathbf{b}^H(F_{r_k}[\tilde{p}])\, \hat{\mathbf{v}}_k^{(i)}\Big\|^2, \tag{154}$$

where $\hat{\mathbf{v}}_k^{(i)}$ plays the same role as $\hat{\mathbf{v}}_k$ in (146), but whose n-th element is defined as (see (145))

$$\hat{v}_k^{(i)}[n] \triangleq \Big[\mathbf{a}^H\Big(\breve{F}_{D_k}^{(i)}\Big)\, \mathbf{a}\Big(\breve{F}_{D_k}^{(i)}\Big)\Big]^T \mathbf{a}^H\Big(\breve{F}_{D_k}^{(i)}\Big)\, \mathbf{H}_n^{(i)}[k] \tag{155}$$

with $\breve{F}_{D_k}^{(i)} \triangleq F_D[\breve{l}_k^{(i)}]$ (see (111)); here, $\mathbf{H}_n^{(i)}[k] \triangleq [\hat{H}_{0,n}^{(i)}[k],\, \hat{H}_{1,n}^{(i)}[k], \ldots,\, \hat{H}_{M-1,n}^{(i)}[k]]^T$. Moreover, the vector $\mathbf{b}(F_{r_k}[\tilde{p}])$ appearing in the RHS of (154) is an N-dimensional column vector whose n-element, denoted $b_n(F_{r_k}[\tilde{p}])$, is defined by (27).

Finally, given $\hat{F}_{r_k}^{(i)} = F_r[\hat{p}_k^{(i)}]$ (see (112)), a finer estimate of the normalized Doppler frequency is evaluated as $\hat{F}_{D_k}^{(i)} = F_D[\hat{l}_k^{(i)}]$, where

$$\hat{l}_k^{(i)} \triangleq \arg \max_{\tilde{l} \in \mathcal{S}_{M_0}} \Big|\mathbf{a}^H\Big(F_D[\tilde{l}]\Big) \hat{\mathbf{B}}\Big(\hat{F}_{r_k}^{(i)}\Big)\Big|^2, \tag{156}$$

and the m-th element ($m = 0, 1, \ldots, M-1$) of the row vector $\hat{\mathbf{B}}(\hat{F}_{r_k}^{(i)})$ is still defined by (148) with $\hat{F}_{r_k}^{(i)}$ in place of $\hat{F}_{r_k}$. This concludes the i-th iteration.

The estimates $\{(\hat{F}_{D_k}^{(N_{\mathrm{REF}})},\, \hat{F}_{r_k}^{(N_{\mathrm{REF}})}, \hat{A}_k^{(N_{\mathrm{REF}})});\ k = 0, 1, ..., \hat{K} - 1\}$ available at the end of the last (i.e., of the N_{REF}-th) iteration represent the output of the refinement algorithm.

It can be shown that the computational cost of MWL algorithm is $\mathcal{O}(N_{\mathrm{MW}})$, where (see [41, Sec. III-E, eq. (44)])

$$N_{\mathrm{MW}} = \bar{N}_{\mathrm{MW}}(M_0, N_0) + N_{\mathrm{REF}}\, \bar{N}_{\mathrm{MW}}(\tilde{M}_0, \tilde{N}_0). \tag{157}$$

Here,

$$\begin{aligned} \bar{N}_{\mathrm{MW}}(M_0, N_0) = \big[&M^2(6N + 8M_0) + 30MN \\ &+ 8N_0N + 30M_0M\big] \end{aligned} \tag{158}$$

represents the cost due to a single iteration of the algorithm; note that the parameters (M_0, N_0) $((\tilde{M}_0, \tilde{N}_0))$ define the grid size for the initialization (for the refinement) step.

4) EM-based algorithm (EM)*:* The EM algorithm can be employed jointly with any of the previously described algorithms to refine their estimates of the parameters of multiple targets. For this reason, generally speaking, we can assume that the EM algorithm is fed by the $\hat{K}$-dimensional vectors $\hat{\mathbf{F}}_D = [\hat{F}_{D_0}, \hat{F}_{D_1}, \ldots, \hat{F}_{D_{\hat{K}-1}}]$, $\hat{\mathbf{F}}_r = [\hat{F}_{r_0}, \hat{F}_{r_1}, \ldots, \hat{F}_{r_{\hat{K}-1}}]$ and $\hat{\mathbf{A}} = [\hat{A}_0, \hat{A}_1, \ldots, \hat{A}_{\hat{K}-1}]$, collecting the initial estimates of the normalised Doppler, normalised delay and the complex amplitude of the $\hat{K}$ detected targets.

The EM algorithm is iterative; in each of its iterations, it executes an *expectation step* (E-step) followed by a *maximisation step* (M-step). In our description of such steps, we focus on the i-th iteration (with $i = 1, ..., N_{\mathrm{REF}}$, where N_{REF} denotes the overall number of iterations) and consider the k-th target (with $k = 0, 1, .., \hat{K} - 1$). At the beginning of this iteration, the estimates $(\hat{F}_{D_k}^{(i-1)}, \hat{F}_{r_k}^{(i-1)}, \hat{A}_k^{(i-1)})$ are available for the normalised Doppler, the normalised delay and the complex amplitude, respectively, of the considered target; note that, if $i = 1$, we have that $(\hat{F}_{D_k}^{(0)}, \hat{F}_{r_k}^{(0)}, \hat{A}_k^{(0)}) = (\hat{F}_{D_k}, \hat{F}_{r_k}, \hat{A}_k)$. The two steps accomplished within the considered iteration are described below.

1) *E step* - In this step, the cost function

$$J_{\mathrm{EM}_k}^{(i)}(l,p) = \frac{1}{MN}\left\| \left(\breve{\mathbf{M}}_k^{(i)}\left(\tilde{F}_{D_k}^{(i)}[l], \tilde{F}_{r_k}^{(i)}[p] \right) \right)^H \hat{\mathbf{H}}_k^{(i)} \right\|^2 \tag{159}$$

is computed for $l = 0, 1, \ldots, M_0 - 1$ and $p = 0, 1, \ldots, N_0 - 1$; here, the $(MN) \times K$ matrix $\breve{\mathbf{M}}_k^{(i)}(\tilde{F}_{D_k}^{(i)}[l], \tilde{F}_{r_k}^{(i)}[p])$ is defined by (131),

$$\hat{\mathbf{H}}_k^{(i)} = \hat{\mathbf{H}}_k^{(i-1)} + \beta_k^{(i)} \left[\bar{\mathbf{H}} - \sum_{k'=0}^{\hat{K}-1} \hat{\mathbf{H}}_{k'}^{(i-1)} \right] \tag{160}$$

is the reconstructed channel vector evaluated for the k-th target in the i-th iteration, $\bar{\mathbf{H}}$ is the (MN)-dimensional vector resulting from the ordered concatenation of the columns of the channel measurement matrix $\hat{\mathbf{H}}_{0,0}$ (48),

$$\hat{\mathbf{H}}_k^{(i-1)} \triangleq \hat{A}_k^{(i-1)}\, \mathbf{M}_k^{(i-1)}, \tag{161}$$

where $\mathbf{M}_k^{(i-1)}$ an MN-dimensional vector defined right after (131). Moreover, for any i, the $\hat{K}$ parameters $\{\beta_k^{(i)}; k = 0, 1, ..., \hat{K} - 1\}$ are the so called *mixing coefficients* and satisfy the inequalities $0 \leqslant \beta_k^{(i)} \leqslant 1$ for $k = 0, 1, ..., \hat{K} - 1$ (e.g., see [41, Par. III-D]).

2) *M step* - The new (and, hopefully, finer) estimates $\hat{F}_{D_k}^{(i)} = F_D[\hat{l}_k^{(i)}]$ and $\hat{F}_{r_k}^{(i)} = F_r[\hat{p}_k^{(i)}]$ of F_{D_k} and F_{r_k}, respectively, are evaluated; here, $(\hat{l}_k^{(i)}, \hat{p}_k^{(i)})$ represents the value of the couple (l, p) maximising the function $J_{\mathrm{EM}_k}^{(i)}[l, p]$ over a specific grid, whose center depends on both $\hat{F}_{D_k}^{(i-1)}$ and $\hat{F}_{r_k}^{(i-1)}$, and whose step size gets smaller as i increases. The grid employed in this case is generated according to the same criteria illustrated for the refined procedure of the CLEAN algorithm (these criteria are described right after (121)).

Finally, the complex amplitude $\hat{A}_k^{(i)}$ is evaluated as (e.g., see [31, Sec IV, eq. 48]):

$$\hat{A}_k^{(i)} = \frac{1}{M\,N} \hat{\mathbf{M}}_k^{(i)}\, \hat{\mathbf{H}}_k^{(i)}. \tag{162}$$

This concludes the M step.

At the end of the last iteration (i.e., for $i = N_{\mathrm{REF}}$), the final estimates $(\hat{F}_{D_k}^{(N_{\mathrm{REF}})}, \hat{F}_{r_k}^{(N_{\mathrm{REF}})}, \hat{A}_k^{(N_{\mathrm{REF}})})$ are available, with $k = 0, 1, \ldots \hat{K} - 1$.

The overall computational cost of a single iteration of the EM algorithm in the presence of $\hat{K}$ targets can be expressed in a similar way as [41, App. C], i.e. as

$$\mathcal{C}_{\mathrm{EM}} = \hat{K}\big(\mathcal{C}_H + \mathcal{C}_{\mathcal{A}} + \mathcal{C}_J + \mathcal{C}_{l,p} + \mathcal{C}_{\breve{M}}\big), \tag{163}$$

where: a) $\mathcal{C}_H = 2(\hat{K} + 2)\, M\, N$ is the contribution due to the computation of $(M\,N)$-dimensional vectors $\{\hat{\mathbf{H}}_k^{(i)}\}$ (see eq. (160)); b) $\mathcal{C}_{\breve{M}} = 6M\,N\,M_0\,N_0$ is the contribution due to the evaluation of the matrix $\breve{\mathbf{M}}_k^{(i)}(\cdot, \cdot)$ (M_0 and N_0 denote the size of the search grid for the normalized Doppler frequency and the normalized delay, respectively); c) $\mathcal{C}_J = 8M\,N\,M_0\,N_0$ ($\mathcal{C}_{l,p} = 4M_0\,N_0$) is the cost due to the computation (optimization) of $J_{\mathrm{EM}_k}^{(i)}[l, p]$ (see (159)); d) $\mathcal{C}_{\mathcal{A}} = 8M\,N$ is the cost due to the computation of the complex amplitude estimation $\hat{A}_k^{(i)}$ on the basis of (162).

The complexities of the estimation algorithms considered in our computer simulations are listed in Table I.

V. Numerical Results

The accuracy of the CSFDEC algorithm and of the other estimation algorithms illustrated in the previous section has been assessed in four different scenarios. The first three scenarios (denoted **S1**, **S2** and **S3**) are characterised by a couple of targets having amplitudes $A_0 = A_1 = 0.8$, but differ for the assumptions we make about target ranges and speeds. More specifically, we have that:

Table I
ORDER OF THE COMPUTATIONAL COMPLEXITY OF VARIOUS ESTIMATION ALGORITHMS.

Algorithm	2D periodogram method	MWL	2D-MUSIC
$\mathcal{O}(\cdot)$	$M_0\,N_0\log_2(M_0\,N_0)$	$\bar{N}_{\rm MW}(M_0,N_0)+N_{\rm REF}\,\bar{N}_{\rm MW}(\tilde{M}_0,\tilde{N}_0)$	$(M\,N+M_0\,N_0)(M\,N)^2$
Algorithm	CSFDEC	CLEAN	MZML
$\mathcal{O}(\cdot)$	$16\,M_0\,N_0\log_2(M_0\,N_0)+K^2\,N_{\rm it}\;16\,I_D\,I_r$	$\bar{N}_{\rm CL}(M_0,N_0)+N_{\rm REF}\,\bar{N}_{\rm CL}\left(\tilde{M}_0,\tilde{N}_0\right)$	$N_{\rm REF}\,8M_0\,N_0\big(K^2+K\big)M^2N^2$
Algorithm	MAP-ML	EM	
$\mathcal{O}(\cdot)$	$N_{\rm REF}\,8\,(M_0+N_0)\,\big(K^2+K\big)\,M^2N^2$	$N_{\rm REF}\big[K(14M\,N\,M_0\,N_0)+2K^2M\,N\big]$	

a) The target ranges (velocities) are $R_0=10$ m and $R_1=35$ m ($v_0=5/3.6$ m/s and $v_1=10/3.6$ m/s) in **S1**.

b) In **S2**, the range R_0 (velocity v_0) is uniformly distributed[12] over the interval $[R_{\min},R_{\max}]=[3,\,80]$ m ($[v_{\min},v_{\max}]=[1/3.6,\,36/3.6]$ m/s), whereas $R_1=R_0+1.1R_{\rm bin}$ and $v_1=v_0+1.1v_{\rm bin}$; here, $R_{\rm bin}=c/(2N\Delta_f)$ ($v_{\rm bin}=c/(2M\,f_c\,T_s)$) represents the size of the range (velocity) bin that characterizes our FFT processing in the absence of oversampling.

c) In **S3**, the range R_0 (velocity v_0) is uniformly distributed over the interval $[R_{\min},R_{\max}]=[3,\,30]$ m ($[v_{\min},v_{\max}]=[1/3.6,\,20/3.6]$ m/s), whereas $R_1=R_0+\Delta_R(d)\,R_{\rm bin}$ ($v_1=v_0+\Delta_v(d)\,v_{\rm bin}$), with $d=0,\,1,\,\ldots,\,10$; here, $\Delta_R(d)$ ($\Delta_v(d)$) represents the tone spacing normalised with respect to $R_{\rm bin}$ ($v_{\rm bin}$). In particular $\Delta_R(d)=0.8+0.05\,d$ ($\Delta_v(d)=0.8+0.05\,d$); moreover, the *signal-to-noise ratio* (SNR), that, in general, is defined as

$$\mathrm{SNR}\triangleq\frac{\sum_{k=0}^{K-1}|A_k|^2}{\sigma_W^2} \tag{164}$$

where σ_W^2 represents the variance of each element of the complex noise sequence $\{\bar{W}_m(n)\}$ (see (28)), is equal to 0 dB in this scenario.

d) The fourth scenario (denoted **S4**) is characterized by $K\in\{2,\,3,\,\ldots,\,9\}$, i.e. by a varying number of targets. For any K, the amplitude, range and velocity of the k-th target are given by

$$A_k\triangleq 10^{-k\Delta_a/10} \tag{165}$$

$R_k\triangleq R_0+1.8\,k\,R_{\rm bin}$ and $v_k\triangleq v_0+1.8\,k\,v_{\rm bin}$, respectively, with $k=0,\,1,\,\ldots,\,K-1$. Moreover, the random variables R_0 and v_0 are generated in the same way as **S3** and the SNR is equal to 5 dB for the strongest tone.

It is important to point out that: a) on the one hand, the study of **S1** has been uniquely motivated by our interest in comparing the accuracy achieved by all the considered algorithms in a simple scenario, characterised by two targets whose spacing in the velocity and range domains is fixed and not small; b) on the other hand, the study of **S2** (**S3**) has allowed us to assess how the considered estimators perform in the presence of two close targets whose spacing in both the range and velocity domains is small and fixed (variable); c) the study of **S4** unveils how the performance of different estimation algorithms is affected by an increasing number of close targets; d) in all the considered scenarios, target velocities are always positive.

In our computer simulations, the estimation accuracy of each algorithm has been assessed by evaluating the *root mean square error* (RMSE) for the range and velocity of the considered targets (these are denoted $RMSE_r$ and $RMSE_v$, respectively) under the assumption that the overall number of targets is known a priori. Moreover, the following parameters have been selected for the OFDM modulation: 1) overall number of subcarriers $N=32$; 2) overall number of OFDM symbols/frame $M=32$; 3) subcarrier spacing $\Delta_f=250$ kHz; 4) cyclic prefix duration $T_G=12.5$ μs (consequently, the OFDM symbol duration is $T_s=1/\Delta_f+T_G=16.5$ μs); 5) carrier frequency $f_c=78$ GHz. Then, we have that $R_{\rm bin}=18.75$ m and $v_{\rm bin}=3.64$ m/s.

In **S1**, the accuracy of eight different estimators (namely, the 2D-FFT[13], 2D-MUSIC, CSFDEC, CLEAN, MWL, MZML, MAP-ML and EM algorithms) has been assessed. Moreover, the following choices have been made for these algorithms[14]: a) the oversampling factor $L_D=16$ ($L_r=16$) has been selected for Doppler (range) estimation in both the 2D-FFT and CSFDEC algorithms (so that $M_0=ML_D=512$ and $N_0=NL_r=512$; see (49) and (50), respectively); b) (74) has been always employed in the evaluation of the CSFDEC residuals (so that 13 DSFTs $\{\bar{\mathbf{Y}}_{k_1,k_2}\}$ have been computed in each new run); c) the 2D-FFT method has been used to compute the initial estimates of the MZML, MAP-ML and EM algorithms; d)$M_0=512$ ($N_0=512$), has been chosen for the refinement grid over Doppler (range) described right after (121) (and employed by the CLEAN, MWL, MZML, MAP-ML and EM algorithms); e) $N_{\rm it}=20$ refinement steps have been accomplished for the

[12]In both **S2** and **S3**, R_0 and v_0 are *independent* random variables.

[13]In this section, the acronym 2D-FFT is used to denote the 2D periodogram method.

[14]The following values of the considered parameters have been also employed in **S2** and **S3**.

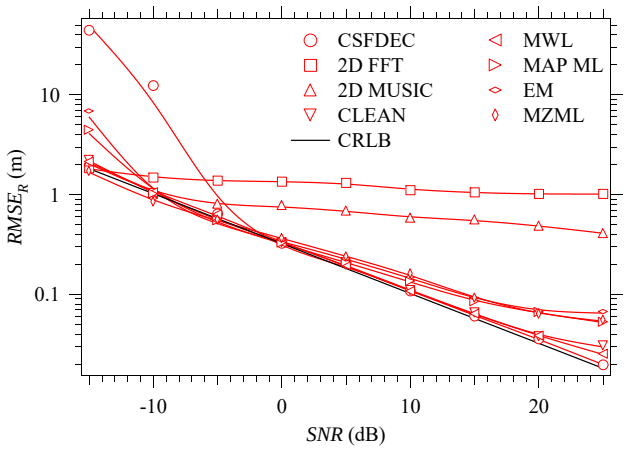

Figure 1. Root mean square error performance achieved in range estimation (first scenario)

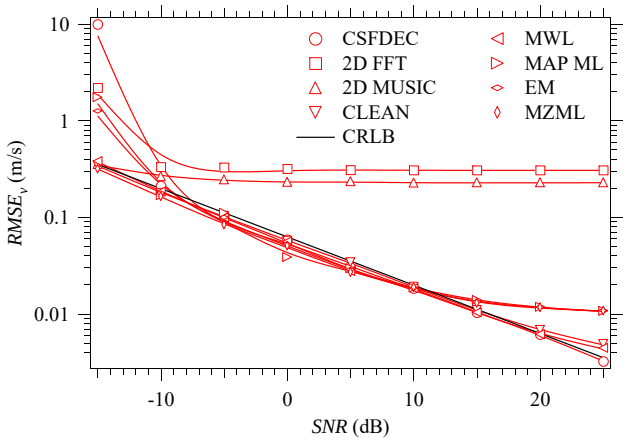

Figure 2. Root mean square error performance achieved in velocity estimation (first scenario)

computation of the residuals in the CSFDEC algorithm and the interpolation[15] orders $I_D = I_r = 7$ have been selected; f) $N_{\rm REF} = 5$ ($N_{\rm REF} = 3$) re-estimations have been executed by the CSFDEC, CLEAN and MWL (MZML, MAP-ML and EM) algorithms; g) $M_0 = N_0 = 11$ ($M_0 = N_0 = 9$) have been chosen for the grid size in the CLEAN and MWL (MZML, MAP-ML and EM) algorithms during the re-estimation steps; h) a unit value has been assigned to the coefficient $\beta_k^{(i)}$ (with $k = 0, 1, \dots K-1$ and $i = 1, 2, \dots N_{\rm REF}$) in the EM algorithm (see (160)). Moreover, in **S1**, $M_0 = 32$ ($N_0 = 61$) has been selected for the number of trial values of the 2D-MUSIC algorithm and for the initial trial values of the CLEAN and MWL algorithms in the Doppler (range) domain. More specifically, uniformly spaced trial values for range (velocity) have been selected in the interval[16] $[0, R_{\rm max}]$ ($[0, v_{\rm max}]$) with $R_{\rm max} = 36$ m ($v_{\rm max} = 3.62$ m/s); the spacing between adjacent values is $\Delta_R = 0.6$ m ($\Delta_v = 0.1166$ m/s).

Some numerical results referring to **S1** are given in Fig. 1 (2), where the $RMSE_r$ ($RMSE_v$) characterising all the considered algorithms is shown for SNR $\in [-15, 25]$ dB; note that, in these figures and in all the following ones, simulation results are represented by labels, whereas continuous lines are drawn to ease reading. From these results it is easily inferred that:

1) The CSFDEC, CLEAN and MWL algorithms achieve good accuracy (very close to the CRLB) thanks to their use of a cancellation and refinement procedure. Note that the computational complexity of the CSFDEC (CLEAN) algorithm is approximately 16 (3.4) times higher than that of the 2D-FFT, whereas that of the MWL algorithm is 2 times lower.
2) Traditional techniques, like the 2D-FFT and 2D-MUSIC algorithms, perform poorly at high SNRs since their estimates suffer from a bias due to the leakage effect. Moreover, the 2D-MUSIC outperforms the 2D-FFT algorithm, but at the price of a 648 times higher complexity.
3) The MAP-ML and the MZML algorithms perform similarly since both aim at maximising the same cost function. Their computational costs are approximately 577 and 2593 times higher than that of the 2D-FFT algorithm.
4) The EM algorithm can be fruitfully exploited to refine the estimates generated by other methods; in particular, if employed

[15]In all our simulations, the *barycentric interpolation* described in [38] has been always used.
[16]In our simulations, positive trial values are always considered for target velocities, without loss of generality.

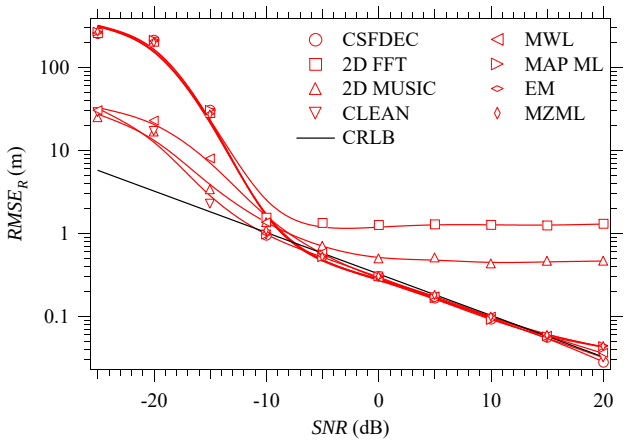

Figure 3. Root mean square error performance achieved in range estimation (second scenario)

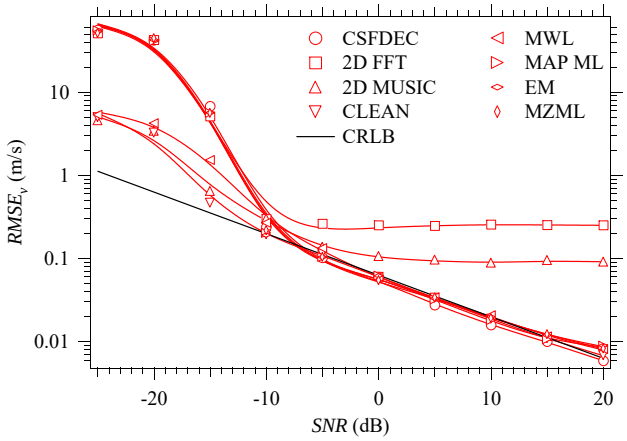

Figure 4. Root mean square error performance achieved in velocity estimation (second scenario)

jointly with the 2D-FFT algorithm, achieves an estimation accuracy similar to that provided by the MAP-ML and MZML algorithms, but at approximately a 233 times smaller computational cost.

Some numerical results referring to **S2** are provided in Fig. 3 (4), where the $RMSE_r$ ($RMSE_v$) characterising all the considered algorithms is shown for SNR $\in [-25, 25]$ dB. In this case, $M_0 = 131$ ($N_0 = 181$) have been selected for the number of trial values of the 2D-MUSIC algorithm and for the initial trial values of the CLEAN and MWL algorithms in the Doppler (range) domain. In particular, uniformly spaced trial values for range (velocity) have been selected in the interval $[0, R_{\max}]$ ($[0, v_{\max}]$) with $R_{\max} = 108$ m ($v_{\max} = 15.15$ m/s); the spacing between adjacent values is $\Delta_R = 0.6$ m ($\Delta_v = 0.1166$ m/s).

These results lead to the following conclusions:

1) The CSFDEC, MWL, CLEAN, MAP-ML, MZML and EM algorithms are substantially more accurate than the 2D-FFT and 2D-MUSIC techniques. In particular, the RMSEs in range (velocity) of the 2D-FFT and 2D-MUSIC algorithms are 3.9 (4) and 1.5 (1.68) times higher, respectively, than that of the above mentioned group of algorithms at SNR $= 0$ dB; moreover, these performance gaps, in terms of both $RMSE_r$ and $RMSE_v$, tend to increase by a factor 1.75 if the SNR is incremented by 5 dB.
2) The trend of both the $RMSE_r$ and $RMSE_v$ curves referring to the 2D-MUSIC and 2D-FFT algorithms does not follow that of the corresponding CRLB; for this reason, these algorithms are ignored in following.
3) The SNR threshold of the CSFDEC, CLEAN, MAP-ML and EM algorithms is about -10 dB, whereas that of the MWL algorithm is substantially higher (about -5 dB).
4) The MAP-ML algorithm performs similarly as the MZML algorithm; since the latter estimator requires an higher computational effort than the former one, it is ignored in the following.

It is also important to point out that the considerations illustrated about the computational complexity of the various algorithms in **S1** still hold; however, the complexities of the CLEAN, MWL, and 2D-MUSIC algorithms are 32 times, 0.66 times and 5497 times, respectively, higher than that of the 2D-FFT algorithm.

In **S3**, the RMSEs have been evaluated for different values of the normalised tone spacing δ_R and δ_v; some numerical results referring to this scenario are illustrated in Figs. 5 and 6, that show the dependence of $RMSE_r$ and $RMSE_v$, respectively,

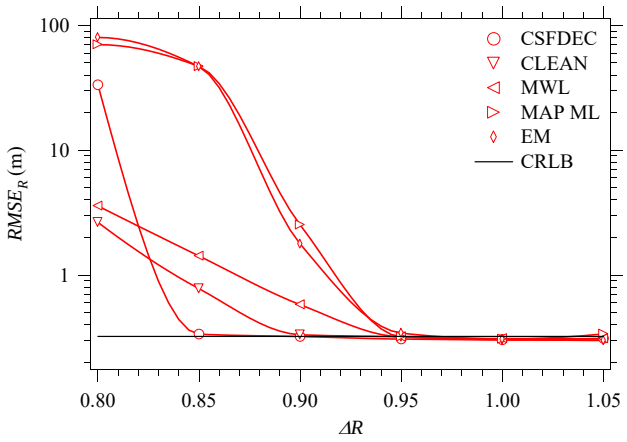

Figure 5. Root mean square error performance achieved in range estimation (third scenario) vs normalized tone spacing δ_R. The CSFDEC, CLEAN, MWL, MAP-ML and EM algorithms are considered.

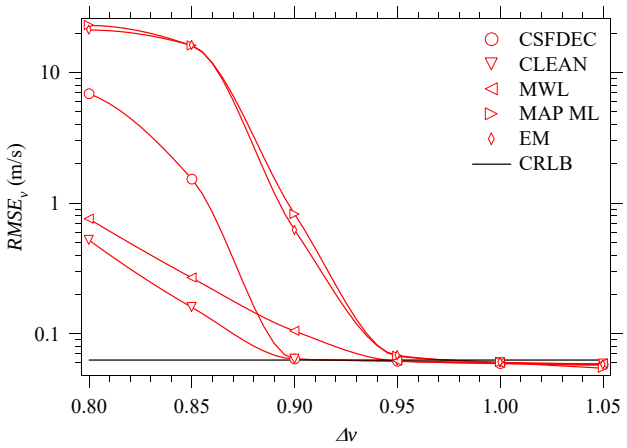

Figure 6. Root mean square error performance achieved in velocity estimation (third scenario) vs normalized tone spacing δ_v. The CSFDEC, CLEAN, MWL, MAP-ML and EM algorithms are considered.

on the normalized tone spacing. In this case, the number of initial trial values are $M_0 = 101$ ($N_0 = 101$) for the CLEAN and MWL algorithms in the Doppler (range) domain. Moreover, uniformly spaced trial values for range (velocity) have been selected in the interval $[0, R_{\max}]$ ($[0, v_{\max}]$) with $R_{\max} = 60$ m ($v_{\max} = 11.66$ m/s) and the spacing between adjacent values is $\Delta_R = 0.6$ m ($\Delta_v = 0.1166$ m/s).

These results lead to the following conclusions:

1) The lowest threshold in range estimation is achieved by the CSFDEC algorithm; more specifically, in the considered scenario, this threshold is found at the normalised spacing $\delta_R(2) = 0.9$.
2) The lowest threshold in velocity estimation is achieved by both the CLEAN and CSFDEC algorithms; note also that the complexity of the CSFDEC is approximately 1.11 times higher than that of the CLEAN algorithm in this case.

Based on the considerations illustrated above, in **S4** we restrict our attention to the CSFDEC, CLEAN, MWL, MAP-ML and EM algorithms. Moreover, our performance analysis does not concern $RMSE_r$ and $RMSE_v$, but the *probability of failure* (P_f), i.e. the probability that a given algorithm does not converge. Our interest in P_f can be motivated as follows. Each of the considered estimation algorithms is highly nonlinear; for this reason, its behavior is characterized by a threshold, whose value depends on the specific scenario in which it is employed and is certainly influenced by the values of SNR and K. In practice, if an estimation algorithm operates above its threshold, failures are very rare events; consequently, the assessed RMSEs are negligibly influenced by them, i.e., they account for the intensity of the errors observed after the convergence of the algorithm itself. On the contrary, if the algorithm operates below its threshold, a portion of its estimation errors (but not all of them) refers to events in which it has not converged; when this happens, large estimation errors (i.e., outliers) may be observed. In the last case, RMSEs are not so meaningful since they account for two heterogeneous contributions. In our computer simulations, we have observed that large estimation errors become more and more frequent as K increases in the considered scenario. To detect the frequency of these errors, we counted, in each simulation run, the number of *failure events* of each of the considered algorithms; in practice, an event of this type is detected whenever the absolute value of the range error

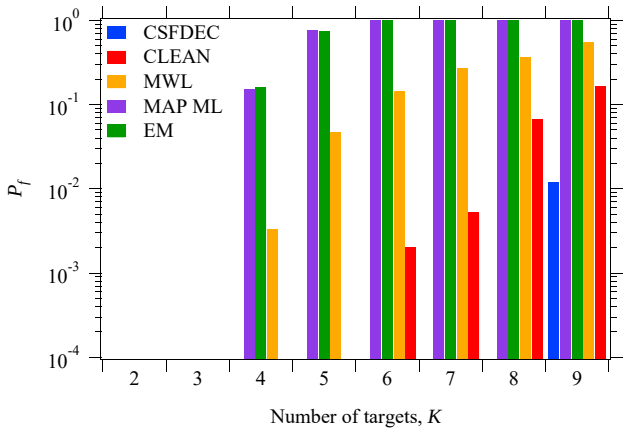

Figure 7. Probability of failure versus overall number of tones (fourth scenario). The CSFDEC, CLEAN, MWL, MAP-ML and EM algorithms are considered.

or that of the velocity error (or both) exceed the thresholds $\Delta\epsilon_r = c/(4N\Delta_f) = 9.375$ m and $\Delta\epsilon_v = c/(4Mf_cT_s) = 1.82$ m/s, respectively[17]. Moreover, in our simulations, the following changes have been made with respect to the other scenarios: a) $N_{\mathrm{REF}} = 7$ ($N_{\mathrm{REF}} = 5$) re-estimations have been executed by the CSFDEC, CLEAN and MWL (MAP-ML and EM) algorithms; b) $M_0 = 551$ ($N_0 = 551$) have been selected for the initial trial values of the CLEAN and MWL algorithms in the Doppler (range) domain. In this case, uniformly spaced trial values for range (velocity) have been selected in the interval $[0, R_{\max}]$ ($[0, v_{\max}]$) with $R_{\max} = 330$ m ($v_{\max} = 64.1$ m/s) and the spacing between adjacent values is $\Delta_R = 0.6$ m ($\Delta_v = 0.1166$ m/s).

The probability of failure estimated for $K = 2, 3, \ldots, 9$ is illustrated in Fig. 7. From this figure it is easily inferred that:

1) The MAP-ML and EM (MWL) algorithms exhibit a P_f greater than 10^{-2} for $K \geq 4$ ($K \geq 5$).
2) The CSFDEC algorithm is substantially more robust than all the other algorithms since it is characterized by a P_f not exceeding 10^{-3} for $K \leq 8$;
3) The CLEAN algorithm achieves a P_f smaller than 10^{-2} for $K \leq 7$.

These results show that the CSFDEC algorithm performs substantially better than the other estimators in the presence of multiple closely spaced targets. This feature plays a fundamental role in the estimation of extended targets, whose radar image is usually a dense point cloud.

Finally, based on all the results illustrated above, we can state that, thanks to its accuracy, its limited complexity and its ability to resolve multiple closely spaced point targets, the CSFDEC algorithm represents a good candidate for target detection and estimation in future OFDM-based radars.

VI. Conclusions

In this manuscript, a novel algorithm, dubbed CSFDE, for the detection of a single 2D complex tone and the estimation of its parameters has been derived. Moreover, it has been shown how combining the CSFDE algorithm with a serial cancellation procedure leads to the development of a new algorithm for the detection and the estimation of multiple 2D tones. Then, the last algorithm, called CSFDEC, has been applied to the detection of multiple targets, and to the estimation of their range and velocity in an OFDM-based radar system. In addition, it has been compared, in terms of accuracy and computational complexity, with other estimation methods available in the technical literature. Our simulation results evidence that the CSFDEC algorithm is very accurate and outperforms all the other related estimators in the presence of multiple closely spaced targets. Future work concerns the application of the CSFDEC algorithm to other JCAS systems.

Appendix

A. Spectral Cancellation of a Two-Dimensional Complex Tone

In this paragraph, the expression of the vector $\bar{\mathbf{C}}_{0,0}(\hat{A}_k^{(i-1)}, \hat{F}_{D_k}^{(i-1)}, \hat{F}_{r_k}^{(i-1)})$ appearing in the RHS of (92) is provided. This vector is evaluated to cancel the contribution of the sequence

$$s_{m,n}\big(\bar{F}_D, \bar{F}_r, \bar{A}\big) = \bar{A}\, \bar{w}_D^m\, \bar{w}_r^n \tag{166}$$

to the vector $\bar{\mathbf{Y}}_{0,0}$ (46) (the adopted cancellation procedure is expressed by (91) and (92)); here,

$$\bar{w}_D \triangleq \exp\big(j2\pi\bar{F}_D\big) \tag{167}$$

[17]Note that $\Delta\epsilon_r$ ($\Delta\epsilon_v$) correspond to half the size of the range (Doppler) bin characterizing the processing of the considered algorithms.

and

$$\bar{w}_r \triangleq \exp(-j2\pi\bar{F}_r). \tag{168}$$

Since $\bar{\mathbf{Y}}_{0,0}$ is the order (M_0, N_0) DSFT of the zero-padded version $\hat{\mathbf{H}}_{0,0}^{(ZP)}$ (47) of the matrix $\hat{\mathbf{H}}_{0,0}$ (48), it is easy to show that

$$\bar{\mathbf{C}}_{0,0}\big(\bar{A}, \bar{F}_D, \bar{F}_r\big) = \bar{A}\,\bar{\mathbf{W}}_0, \tag{169}$$

where $\bar{\mathbf{W}}_0$ denotes the order (M_0, N_0) DSFT of the $M_0 \times N_0$ matrix

$$\bar{\mathbf{w}}_0 \triangleq \begin{bmatrix} \bar{\mathbf{w}} & \mathbf{0}_{M,N_0-N} \\ \mathbf{0}_{M_0-M,N} & \mathbf{0}_{M_0-M,N_0-N} \end{bmatrix}, \tag{170}$$

$\bar{\mathbf{w}} \triangleq [w_{m,n}]$ is an $M \times N$ matrix such that

$$w_{m,n} \triangleq \bar{w}^{m-n}, \tag{171}$$

with $m = 0, 1, ..., M-1$ and $n = 0, 1, ..., N-1$, and $\bar{w} \triangleq \bar{w}_D\,\bar{w}_r$. Then, the (m,n)-th element of the matrix $\bar{\mathbf{W}}_0$ is given by

$$\begin{aligned} \bar{W}_0[m,n] &= \frac{1}{M_0}\sum_{l=0}^{M-1} \bar{w}_D^l \exp\!\left(-j2\pi\frac{m}{M_0}l\right) \\ &\quad\cdot\frac{1}{N_0}\sum_{p=0}^{N-1} \bar{w}_r^p \exp\!\left(j2\pi\frac{n}{N_0}p\right) \\ &= \frac{1}{M_0}\sum_{l=0}^{M-1} (\hat{q}_D[m])^l \frac{1}{N_0}\sum_{p=0}^{N-1} (\hat{q}_r[n])^p, \end{aligned} \tag{172}$$

where $\hat{q}_D[m] \triangleq \exp(j2\pi(\hat{F}_D - m/M_0))$ and $\hat{q}_r[m] \triangleq \exp(-j2\pi(\hat{F}_r - n/N_0))$. Finally, it is useful to note that the identity

$$\sum_{n=0}^{N-1} q^n = \frac{q^N - 1}{q - 1}, \tag{173}$$

holding for any $q \in \mathbb{C}$, can be exploited for an efficient computation of the two sums appearing in the RHS of (172).

B. Cancellation of Two-Dimensional Spectral Leakage

In this paragraph, the expression of the quantity $\bar{Y}_{k_1,k_2}(\hat{F}_{D,c_i}^{(i)}, \hat{F}_{r,c_i}^{(i)}; \hat{A}_k^{(i-1)}, \hat{F}_{D_k}^{(i-1)}, \hat{F}_{r_k}^{(i-1)})$ appearing in the RHS of (97) and (101) is derived. This quantity is computed by the CSFDEC algorithm to cancel the contribution of the sequence $\{s_{m,n}(\bar{F}_{D_k}, \bar{F}_{r_k}, \bar{A}_k)\}$ (see (166)) to $\bar{Y}_{k_1,k_2}^{(i)}(\rho_D^{(i)}, \rho_r^{(i)})$ (98) for $k_1, k_2 = 0, 1, 2, 3$. It is not difficult to show that

$$\begin{aligned} &\bar{Y}_{k_1,k_2}\Big(\hat{F}_{D,c_i}^{(i)}, \hat{F}_{r,c_i}^{(i)}; \hat{A}_k^{(i-1)}, \hat{F}_{D_k}^{(i-1)}, \hat{F}_{r_k}^{(i-1)}\Big) \\ &= \bar{A}_k^{(i-1)}\,\bar{W}_{k_1k_2}^{(k)}\Big(\hat{F}_{D,c_i}^{(i)}, \hat{F}_{r,c_i}^{(i)}; \hat{F}_{D_k}^{(i-1)}, \hat{F}_{r_k}^{(i-1)}\Big), \end{aligned} \tag{174}$$

where

$$\begin{aligned} &\bar{W}_{k_1k_2}^{(k)}\Big(\hat{F}_{D,c_i}^{(i)}, \hat{F}_{r,c_i}^{(i)}; \hat{F}_{D_k}^{(i-1)}, \hat{F}_{r_k}^{(i-1)}\Big) \\ &= \frac{1}{M_0}\sum_{m=0}^{M-1} m^{k_1}\Big(\bar{q}_D\Big(\hat{F}_{D,c_i}^{(i)}, \hat{F}_{D_k}^{(i-1)}\Big)\Big)^m \\ &\quad\cdot\frac{1}{N_0}\sum_{n=0}^{N-1} n^{k_2}\Big(\bar{q}_r\Big(\hat{F}_{r,c_i}^{(i)}, \hat{F}_{r_k}^{(i-1)}\Big)\Big)^n, \end{aligned} \tag{175}$$

$$\bar{q}_D\Big(\hat{F}_{D,c_i}^{(i)}, \hat{F}_{D_k}^{(i-1)}\Big) = \exp\Big(j2\pi\Big(\hat{F}_{D_k}^{(i-1)} - \hat{F}_{D,c_i}^{(i)}\Big)\Big), \tag{176}$$

$$\bar{q}_r\Big(\hat{F}_{r,c_i}^{(i)}, \hat{F}_{r_k}^{(i-1)}\Big) = \exp\Big(-j2\pi\Big(\hat{F}_{r_k}^{(i-1)} - \hat{F}_{r,c_i}^{(i)}\Big)\Big), \tag{177}$$

and $\hat{F}_{D_k}^{(i-1)}$ and $\hat{F}_{r_k}^{(i-1)}$ are the *fine estimates* of the normalised Doppler frequency and normalised delay, respectively, computed at the $(i-1)$-th iteration for the k-th target. Note that the identities (173),

$$(q-1)^2\sum_{n=0}^{N-1} n\,q^n = (N-1)\,q^{N+1} - N\,q^N + q, \tag{178}$$

$$(q-1)^3\sum_{n=0}^{N-1} n^2\,q^n = (N-1)^2\,q^{N+2} + N^2\,q^N - q^2 \\ -q - \left(2\,N^2 - 2\,N - 1\right)q^{N+1} \tag{179}$$

and

$$(q-1)^4\sum_{n=0}^{N-1} n^3\,q^n = q + 4q^2 + q^3 - N^3q^N \\ +\left(3N^3 - 3N^2 - 3N - 1\right)q^{N+1} \\ +\left(-3N^3 + 6N^2 - 4N\right)q^{N+2} \\ +(N-1)^3q^{N+3} \tag{180}$$

holding for any $q \in \mathbb{C}$, can be exploited for an efficient computation of all the factors appearing in the RHS of (97) and (98) (with $k_1, k_2 = 0, 1, 2, 3$).

C. Computational Complexity of the CSFDE Algorithm

In this Appendix, the derivation of the approximation (107) of $\mathcal{C}_{\mathrm{CSFDE}}$ is sketched. The evaluation of $\mathcal{C}_{\mathrm{CSFDE}}$ requires that of the computational costs $\mathcal{C}_0(\mathrm{CSFDE})$ and $\mathcal{C}_i(\mathrm{CSFDE})$ appearing in the RHS of (104). The cost $\mathcal{C}_0(\mathrm{CSFDE})$ can be easily estimated on the basis of (105) since: 1) the cost $\mathcal{C}_{\hat{l},\hat{p}}$ is equal to $5M_0N_0 + 2$ (see (81)); 2) the cost[18] $\mathcal{C}_{\bar{\mathbf{Y}}_{k_1,k_2}}$ is equal to $16\,M_0\,N_0\log_2(M_0\,N_0)$ ($13\,M_0\,N_0\log_2(M_0\,N_0)$) if 16 (13) DSFT of order (M_0, N_0) are evaluated, i.e. if (69) ((74)) is employed in the evaluation of $\hat{\Omega}$ and $\hat{\Delta}$; 3) both $\mathcal{C}_{\hat{\Omega}}$ and $\mathcal{C}_{\hat{\Delta}}$ are negligible, being equal to 134 (102) flops if (69) ((74)) is employed in the evaluation of $\hat{\Omega}$ and $\hat{\Delta}$. Substituting these results in the RHS of (105) and keeping the dominant terms only leads to the conclusion that

$$\mathcal{C}_0(\mathrm{CSFDE}) \approx 16\,M_0\,N_0\log_2(M_0\,N_0). \tag{181}$$

Similarly, the cost $\mathcal{C}_i(\mathrm{CSFDE})$ can be easily estimated on the basis of (106), since: 1) the cost $\mathcal{C}_{\bar{Y}}$ is in the order of $25MN$ (I_DI_r) if the evaluation of $\bar{Y}(\hat{F}_D, \hat{F}_r)$ is based on (41) (on the interpolation of multiple elements of the matrix $\bar{\mathbf{Y}}_s$ (54)); 2) the cost $\mathcal{C}_{\bar{Y}_{k_1,k_2}}$ is equal to $15\,\mathcal{C}_{\bar{Y}}$ ($12\,\mathcal{C}_{\bar{Y}}$) if (69) ((74)) is adopted in the evaluation of $\hat{\Omega}$ and $\hat{\Delta}$; 3) the other costs are negligible. The last results lead easily to the conclusion that

$$\mathcal{C}_i(\mathrm{CSFDE}) \approx 16\,I_DI_r, \tag{182}$$

if (69) is employed and 2D interpolation is employed in the evaluation of $\bar{Y}_{k_1,k_2}(\hat{\rho}_D^{(i-1)}, \hat{\rho}_r^{(i-1)})$ (98). Finally, substituting the RHSs of (181) and (182) in that of (104) yields (107).

D. Cramer-Rao Lower Bounds

Cramer-Rao lower bounds (CRLBs) for OFDM-based radar systems have been already derived in [27, Sec V-A, eq. (46)-(47)] and [26, Sec IV-B, eq. (18)-(19)], but refer to Doppler and range only. In our work, CRLBs have been derived for the ML estimation problem (32) investigated in Paragraph III-A. The procedure we followed is conceptually the same as that adopted in [47]; for this reason, the inverse of the Fisher information matrix

$$\mathrm{E}\left\{\frac{\partial L\left(\hat{\mathbf{H}}_{0,0}|\theta\right)}{\partial\theta}\left(\frac{\partial L\left(\hat{\mathbf{H}}_{0,0}|\theta\right)}{\partial\theta}\right)^H\right\}, \tag{183}$$

has been evaluated; here, $\theta \triangleq [F_D, F_r\,, a, \phi]^T$ is the vector collecting the parameters to be estimated ($a = |A|$ and ϕ denote the modulus and the phase, respectively, of the complex amplitude A of the 2D-tone; see (29)), $\hat{\mathbf{H}}_{0,0}$ is the $M \times N$ matrix defined by (48) (its element $\hat{H}_{m,n}$ is expressed by (31)), $L(\cdot|\cdot)$ is the *log-likelihood* function

$$L\left(\hat{\mathbf{H}}_{0,0}\middle|\tilde{\theta}\right) = K_L - MN\ln\sigma_W^2 - \frac{1}{\sigma_W^2} \\ \cdot\sum_{m=0}^{M-1}\sum_{n=0}^{N-1}\varepsilon_{m,n}\left(\tilde{F}_D, \tilde{F}_r, \tilde{a}\exp\left(j\tilde{\phi}\right)\right) \tag{184}$$

$\tilde{\theta} \triangleq [\tilde{F}_D, \tilde{F}_r\,, \tilde{a}, \tilde{\phi}]^T$, K_L is a constant, σ_W^2 is the variance of the noise samples $\{\bar{W}_m(n)\}$ (see (28)) and $\varepsilon_{m,n}(\cdot,\cdot,\cdot)$ is defined by (34) (note that the last quantity depends on the measurements $\{\hat{H}_{m,n}\}$).

[18]Note that this cost includes the computation of the spectrum $\bar{\mathbf{Y}}_{0,0}$ (see (46)).

The CRLBs derived for the estimation of F_D, F_r, a and ϕ are

$$\mathrm{CRLB}_{F_D}(M,N,\mathrm{SNR}) = \frac{3}{2\pi^2 \mathrm{SNR}\, M\,(M^{\,2}-1)\,N}, \tag{185}$$

$$\mathrm{CRLB}_{F_r}(M,N,\mathrm{SNR}) = \frac{3}{2\pi^2 \mathrm{SNR}\, M\;N\,(N^{\,2}-1)}, \tag{186}$$

$$\mathrm{CRLB}_{a}\big(M,N,\sigma_W^2\big) = \frac{\sigma_W^2}{2\,M\,N} \tag{187}$$

and

$$\mathrm{CRLB}_{\phi}(M,N,\mathrm{SNR}) = \frac{7\,M\,N\;+M\;+N-5}{2\,\mathrm{SNR}\,M\,(M+1)\,N\,(N+1)}, \tag{188}$$

respectively, where $\mathrm{SNR} \triangleq a^2/\sigma_W^2$ is the *signal-to-noise ratio* referring to the signal model (31).

Finally, it is worth pointing out that: a) the bounds (185), (186) and (188) are inversely proportional to the SNR, whereas the bound (187) is directly proportional to the noise variance σ_W^2, but independent of the amplitude a; b) the bounds (185) and (186) are identical to those provided in [27, Sec V-A] and [26, Sec IV-B], even if the expressions illustrated in first reference refer to $\omega_{d1} = 2\pi F_D$ and $\omega_{\tau 1} = 2\pi F_r$, whereas those provided in the second one to target speed and range (see eqs. (46)-(47) of [27, Sec V-A] and eqs. (18)-(19) of [26, Sec IV-B], respectively).

REFERENCES

[1] J. A. Zhang, F. Liu, C. Masouros, R. W. Heath, Z. Feng, L. Zheng, and A. Petropulu, "An Overview of Signal Processing Techniques for Joint Communication and Radar Sensing," *IEEE J. Sel. Topics Signal Process.*, vol. 15, no. 6, pp. 1295–1315, Nov. 2021.

[2] P. Kumari, J. Choi, N. Gonzalez-Prelcic, and R. W. Heath, "IEEE 802.11ad-Based Radar: An Approach to Joint Vehicular Communication-Radar System," *IEEE Trans. Veh. Technol.*, vol. 67, no. 4, pp. 3012–3027, Apr. 2018.

[3] C. Sturm and W. Wiesbeck, "Waveform Design and Signal Processing Aspects for Fusion of Wireless Communications and Radar Sensing," *Proc. of the IEEE*, vol. 99, no. 7, pp. 1236–1259, Jul. 2011.

[4] K. V. Mishra, M. Bhavani Shankar, V. Koivunen, B. Ottersten, and S. A. Vorobyov, "Toward Millimeter-Wave Joint Radar Communications: A Signal Processing Perspective," *IEEE Signal Process. Mag.*, vol. 36, no. 5, pp. 100–114, Sep. 2019.

[5] C. Sturm, T. Zwick, and W. Wiesbeck, "An OFDM System Concept for Joint Radar and Communications Operations," in *VTC Spring 2009 - IEEE 69th IEEE Veh. Technol. Conf.* Barcelona, Spain: IEEE, Apr. 2009, pp. 1–5.

[6] M. L. Rahman, J. A. Zhang, X. Huang, Y. J. Guo, and R. W. Heath, "Framework for a Perceptive Mobile Network Using Joint Communication and Radar Sensing," *IEEE Trans. Aerosp. Electron. Syst.*, vol. 56, no. 3, pp. 1926–1941, Jun. 2020.

[7] J. A. Zhang, A. Cantoni, X. Huang, Y. J. Guo, and R. W. Heath, "Framework for an Innovative Perceptive Mobile Network Using Joint Communication and Sensing," in *2017 IEEE 85th IEEE Veh. Technol. Conf.* Sydney, NSW: IEEE, Jun. 2017, pp. 1–5.

[8] J. A. Zhang, X. Huang, Y. J. Guo, and M. L. Rahman, "Signal stripping based sensing parameter estimation in perceptive mobile networks," in *2017 IEEE-APS Top. Conf. on Antennas and Propag. in Wireless Commun. (APWC)*. Verona: IEEE, Sep. 2017, pp. 67–70.

[9] L. Zheng and X. Wang, "Super-Resolution Delay-Doppler Estimation for OFDM Passive Radar," *IEEE Trans. Signal Process.*, vol. 65, no. 9, pp. 2197–2210, May 2017.

[10] J. Capon, "High-resolution frequency-wavenumber spectrum analysis," *Proc. of the IEEE*, vol. 57, no. 8, pp. 1408–1418, 1969.

[11] J. Li and P. Stoica, "An adaptive filtering approach to spectral estimation and SAR imaging," *IEEE Trans. Signal Process.*, vol. 44, no. 2, pp. 1469–1484, 1996.

[12] M. F. Keskin, H. Wymeersch, and V. Koivunen, "ICI-Aware Parameter Estimation for MIMO-OFDM Radar via Apes Spatial Filtering," in *ICASSP 2021 - 2021 IEEE Int. Conf. on Acoust., Speech and Signal Process. (ICASSP)*. IEEE, Jun. 2021, pp. 8248–8252.

[13] ——, "MIMO-OFDM Joint Radar-Communications: Is ICI Friend or Foe?" *IEEE J. Sel. Topics Signal Process.*, vol. 15, no. 6, pp. 1393–1408, Nov. 2021.

[14] T. Yardibi, J. Li, P. Stoica, M. Xue, and A. B. Baggeroer, "Source Localization and Sensing: A Nonparametric Iterative Adaptive Approach Based on Weighted Least Squares," *IEEE Trans. Aerosp. Electron. Syst.*, vol. 46, no. 1, p. 19, 2010.

[15] S. Mercier, S. Bidon, D. Roque, and C. Enderli, "Comparison of Correlation-Based OFDM Radar Receivers," *IEEE Trans. Aerosp. Electron. Syst.*, vol. 56, no. 6, pp. 4796–4813, Dec. 2020.

[16] X. Liu, T. Zhang, Q. Shi, and L. Kong, "CP-OFDM radar range reconstruction in a chaotic Doppler disturbed scenario," in *2020 IEEE Radar Conference (RadarConf20)*. IEEE, Sep. 2020, pp. 1–5, florence, Italy.

[17] Y. L. Sit, C. Sturm, and T. Zwick, "Doppler estimation in an OFDM joint radar and communication system," *2011 German Microw. Conf.*, p. 4, 2011.

[18] D. Roque and S. Bidon, "Range Migration in Symbol-Based OFDM Radar Receivers," in *2021 IEEE 22nd Int. Workshop on Signal Process. Adv. in Wireless Commun. (SPAWC)*, ser. SPAWC. IEEE, 2021, pp. 496–500.

[19] S. Mercier, D. Roque, and S. Bidon, "Study of the Target Self-Interference in a Low-Complexity OFDM-Based Radar Receiver," *IEEE Trans. Aerosp. Electron. Syst.*, vol. 55, no. 3, pp. 1200–1212, Jun. 2019.

[20] G. Liu, H. Niu, M. Zheng, D. Bao, J. Cai, G. Qin, B. Wu, P. Li, and N. Liu, "Integration of Communication and SAR Radar Based on OFDM with Channel Estimation in High Speed Scenario," in *IGARSS 2019 - 2019 IEEE Int. Geoscience and Remote Sens. Symp.* IEEE, Jul. 2019, pp. 2519–2522, yokohama, Japan.

[21] Y. Zeng, Y. Ma, and S. Sun, "Joint Radar-Communication: Low Complexity Algorithm and Self-Interference Cancellation," in *2018 IEEE Global Commun. Conf. (GLOBECOM)*, Dec. 2018, pp. 1–7, abu Dhabi, United Arab Emirates.

[22] J. B. Sanson, D. Castanheira, A. Gameiro, and P. P. Monteiro, "Fusion of Radar and Communication Information for Tracking in OFDM Automotive Radar at 24 GHz," in *2020 IEEE/MTT-S International Microwave Symposium (IMS)*. IEEE, Aug. 2020, pp. 1153–1156, los Angeles, CA, USA.

[23] S. Schieler, C. Schneider, C. Andrich, M. Döbereiner, J. Luo, A. Schwind, R. S. Thomä, and G. Del Galdo, "OFDM waveform for distributed radar sensing in automotive scenarios," *Int. Journal of Microw. and Wireless Technol.*, vol. 12, no. 8, pp. 716–722, Oct. 2020.

[24] S. Mercier, D. Roque, S. Bidon, and C. Enderli, "Correlation-Based Radar Receivers with Pulse-Shaped OFDM Signals," in *2020 IEEE Radar Conf. (RadarConf20)*. IEEE, Sep. 2020, pp. 1–6, florence, Italy.

[25] J. Fink, M. Braun, and F. K. Jondral, "Effects of Arbitrarily Spaced Subcarriers on Detection Performance in OFDM Radar," in *2012 IEEE IEEE Veh. Technol. Conf (VTC Fall)*. IEEE, Sep. 2012, pp. 1–5.

[26] M. Braun, C. Sturm, and F. K. Jondral, "On the single-target accuracy of OFDM radar algorithms," in *2011 IEEE 22nd Int. Symp. on Pers., Indoor and Mobile Radio Commun.* IEEE, Sep. 2011, pp. 794–798.

[27] R. Xie, D. Hu, K. Luo, and T. Jiang, "Performance Analysis of Joint Range-Velocity Estimator With 2D-MUSIC in OFDM Radar," *IEEE Trans. Signal Process.*, vol. 69, pp. 4787–4800, 2021.

[28] Y. Liu, G. Liao, Y. Chen, J. Xu, and Y. Yin, "Super-Resolution Range and Velocity Estimations With OFDM Integrated Radar and Communications Waveform," *IEEE Trans. Veh. Technol.*, vol. 69, no. 10, pp. 11 659–11 672, Oct. 2020.

[29] D. H. N. Nguyen and R. W. Heath, "Delay and Doppler processing for multi-target detection with IEEE 802.11 OFDM signaling," in *2017 IEEE Int. Conf. on Acoust., Speech and Signal Process. (ICASSP)*, Mar. 2017, pp. 3414–3418.

[30] F. Zhang, Z. Zhang, and W. Yu, "Joint Range and Doppler Estimation with Amplitude Weighted Linearly Constrained Minimum Variance Method for OFDM-based RadCom Systems," in *2020 IEEE Radar Conf. (RadarConf20)*, ser. RadarConf20. IEEE, Sep. 2020, pp. 1–6, florence, Italy.

[31] F. Zhang, Z. Zhang, W. Yu, and T.-K. Truong, "Joint Range and Velocity Estimation With Intrapulse and Intersubcarrier Doppler Effects for OFDM-Based RadCom Systems," *IEEE Trans. Signal Process.*, vol. 68, pp. 662–675, 2020.

[32] U. Singh, R. Mitra, V. Bhatia, and A. Mishra, "Target Range Estimation in OFDM Radar System via Kernel Least Mean Square Technique," in *Int. Conf. on Radar Systems (Radar 2017)*. Institution of Engineering and Technology, 2017.

[33] U. Singh, Y. Bhatia, and A. Mishra, "Delay and Doppler Shift Estimation for non-Constant Envelope Modulation in OFDM Radar System," in *Int. Conf. on Radar Systems (Radar 2017)*. Institution of Engineering and Technology, 2017, belfast, UK.

[34] A. El Assaad, M. Krug, and G. Fischer, "Distance and vehicle speed estimation in OFDM multipath channels," in *2016 21st Int. Conf. on Microwave, Radar and Wireless Commun. (MIKON)*. IEEE, May 2016, pp. 1–5.

[35] I. Ziskind and M. Wax, "Maximum likelihood localization of multiple sources by alternating projection," *IEEE Trans. Acoust., Speech, Signal Process.*, vol. 36, no. 10, pp. 1553–1560, Oct. 1988.

[36] D. Rife and R. Boorstyn, "Single tone parameter estimation from discrete-time observations," *IEEE Trans. Inf. Theory*, vol. 20, no. 5, pp. 591–598, Sep. 1974.

[37] E. Isaacson and H. B. Keller, ***Analysis of numerical methods***. New York: Dover Publications, 1994.

[38] J.-P. Berrut and L. N. Trefethen, "Barycentric Lagrange Interpolation," *SIAM Review*, vol. 46, no. 3, pp. 501–517, Jan. 2004.

[39] P. Di Viesti, A. Davoli, G. Guerzoni, and G. M. Vitetta, "Novel Methods for Approximate Maximum Likelihood Estimation of Multiple Superimposed Undamped Tones and Their Application to Radar Systems," Techrxiv, preprint, Aug. 2021.

[40] ——, "Novel Deterministic Detection and Estimation Algorithms for Colocated Multiple-Input Multiple-Output Radars," *IEEE Access*, vol. 10, pp. 2216–2255, 2022.

[41] E. Sirignano, A. Davoli, G. M. Vitetta, and F. Viappiani, "A Comparative Analysis of Deterministic Detection and Estimation Techniques for MIMO SFCW Radars," *IEEE Access*, vol. 7, pp. 129 848–129 861, 2019.

[42] A. Davoli, E. Sirignano, and G. M. Vitetta, "Three-Dimensional Deterministic Detection and Estimation Algorithms for MIMO SFCW Radars," in *2020 IEEE Radar Conf. (RadarConf20)*. IEEE, Sep. 2020, pp. 1–6, florence, Italy.

[43] J. Wang, W. Sun, L. Huang, and J. Zhang, "Accurate and Computationally Efficient Interpolation-based Method for Two-dimensional Harmonic Retrieval," *Digital Signal Processing*, vol. 78, pp. 108–120, 2018.

[44] V. Popović-Bugarin and S. Djukanović, "A Low Complexity Model Order and Frequency Estimation of Multiple 2-D Complex Sinusoids," *Digital Signal Processing*, vol. 104, p. 102794, 2020.

[45] A. Jakobsson, A. Swindlehurst, and P. Stoica, "Subspace-based Estimation of Time Delays and Doppler Shifts," *IEEE Trans. Signal Process.*, vol. 46, no. 9, pp. 2472–2483, Sep. 1998.

[46] C. R. Berger, B. Demissie, J. Heckenbach, P. Willett, and S. Zhou, "Signal Processing for Passive Radar Using OFDM Waveforms," *IEEE J. Sel. Topics Signal Process.*, vol. 4, no. 1, pp. 226–238, Feb. 2010.

[47] Ying-Xian Yao and S. Pandit, "Cramer-Rao lower bounds for a damped sinusoidal process," *IEEE Trans. Signal Process.*, vol. 43, no. 4, pp. 878–885, Apr. 1995.